Green Chemistry Letters and Reviews

ISSN: (Print) (Online) Journal homepage: www.tandfonline.com/journals/tgcl20

Fabrication and characterization of CuO–SiO_2/PVA polymer nanocomposite for effective wastewater treatment and prospective biological applications

Muhammad Yaseen, Abbas Khan, Muhammad Humayun, Shaista Bibi, Saima Farooq, Mohamed Bououdina & Sajjad Ahmad

To cite this article: Muhammad Yaseen, Abbas Khan, Muhammad Humayun, Shaista Bibi, Saima Farooq, Mohamed Bououdina & Sajjad Ahmad (2024) Fabrication and characterization of CuO–SiO_2/PVA polymer nanocomposite for effective wastewater treatment and prospective biological applications, Green Chemistry Letters and Reviews, 17:1, 2321251, DOI: 10.1080/17518253.2024.2321251

To link to this article: https://doi.org/10.1080/17518253.2024.2321251

Published online: 23 Feb 2024.

GREEN CHEMISTRY LETTERS AND REVIEWS
2024, VOL. 17, NO. 1, 2321251
https://doi.org/10.1080/17518253.2024.2321251

Fabrication and characterization of CuO–SiO_2/PVA polymer nanocomposite for effective wastewater treatment and prospective biological applications

Muhammad Yaseen[a], Abbas Khan [a,b], Muhammad Humayun [b], Shaista Bibi[a], Saima Farooq[c], Mohamed Bououdina[b] and Sajjad Ahmad[d]

[a]Department of Chemistry, Abdul Wali Khan University Mardan, Mardan, Pakistan; [b]Energy, Water and Environment Lab, College of Humanities and Sciences, Prince Sultan University, Riyadh, Saudi Arabia; [c]Department of Biological Sciences and Chemistry, College of Arts and Sciences, University of Nizwa, Nizwa, Oman; [d]Department of Zoology, Abdul Wali Khan University Mardan, Mardan, Pakistan

ABSTRACT

The quality of water significantly affects the health and walefare of all orginisms, highlighting the importance to develop low-cost and efficient wastewater treatment methods. Herein, we report the fabrication, characterization, and utilization of a polymer-based ternary nanocomposite (CuO–SiO_2/PVA) for the removal of Nile Blue (NB) and Methylene Blue (MB) contaminants from wastewater, along with exploring its potential biological activities. We have successfully employed the cost-effective sol–gel and in-situ polymerization approaches to fabricate the CuO–SiO_2/PVA based ternary composite, utilizing $Cu(NO_3)_2{\cdot}3H_2O$:Glycerol:TEOS:PVA in a ratio of 8:2:3:4. The desired fabrication of nanocomposite was confirmed through UV-Visible spectroscopy, SEM (scanning electron microscope), TEM (transmission electron microscope), EDX (energy dispersive X-ray diffraction), FTIR (Fourier transform infrared), DSC (differential scanning calorimetry), and TGA (thermogravimetric analysis). In addition to its biological potentialthe performance of the nanocomposite in catalytic / photocatalytic removal of NB and MB dyes is investigated and compared. The higher photodegradation performance of the composite for NB (85%) dye than for MB (76%) dye indicates that variables such as chemical structure, charge, molecular mass, and pH sensitivity of the dyes can influence the catalyst's removal potential. This composite is considered to have a higher capability for removing pollutants and microorganisms from wastewater.

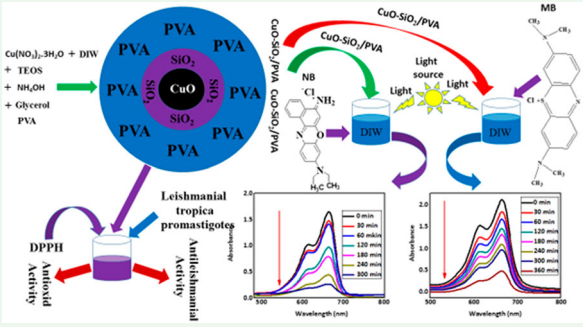

ARTICLE HISTORY
Received 20 July 2023
Accepted 15 February 2024

KEYWORDS
Cuo–SiO_2/PVA; catalysis; photocatalysis; antioxidant and antileishmanial activity

1. Introduction

Water pollution is the contamination of water with chemicals or other foreign elements that harm living organisms (*1*). Water is a crucial resource that has been contaminated by the penetration of numerous contaminants such as dyes, aromatics, drugs, animal waste, and rotten plants by means of various activities. Examples of organic pollutants include pesticides, polychlorinated biphenyls (PCBs), fertilizers from agricultural runoff, phenolic chemicals from chemical or industrial waste, and solid or liquid residues. Inorganic pollutants include, for instance, cadmium (Cd), arsenic (As), mercury (Hg), lead (Pb), chromium (Cr), and other heavy metals (*1*). The use of aromatics, dyes, and other

CONTACT Muhammad Humayun mhumayun@psu.edu.sa Energy, Water and Environment Lab, College of Humanities and Sciences, Prince Sultan University, Riyadh 11586, Saudi Arabia; Abbas Khan abbas80@awkum.edu.pk Department of Chemistry, Abdul Wali Khan University Mardan, Mardan 23200, Pakistan; Energy, Water and Environment Lab, College of Humanities and Sciences, Prince Sultan University, Riyadh 11586, Saudi Arabia

pollutants has been rising globally (2). These organic compounds are used in cosmetics, pharmaceuticals, and food. Azo dyes, which are widely used in food coloring, are well-known for their durability and low cost. To ensure the safety of drinking water and protect public health, regulatory bodies in various countries establish specific limits for contaminants. According to guidelines from the World Health Organization (WHO) and the Environmental Protection Agency (EPA), many organic dyes exhibit noticeable coloration in water even at concentrations below 0.01 mg/L. Consequently, water exceeding this level may not be suitable for consumption. Typically, acceptable limits for industrial discharge range from 0.01 to 0.05 mg/L for most of the organic dyes.

On the other hand, several of these colors can be harmful to living organisms, emphasizing the importance of controlling the level of these sorts of colors in food. Furthermore, because they are poisonous and carcinogenic, they cause genetic mutations, making it critical to remove them from discharges and other water sources (3). Because some contaminants are difficult to remove from wastewater, numerous procedures, both biological and chemical, have been used to remove these contaminants and make the wastewater potable. Because biological procedures are time consuming, they do not meet the requirements for the removal of these effluent, hence chemical remedies have been employed. Various mechanisms are employed in chemical processes, for example electrochemical, advanced oxidation process (AOP), reduction, ozonation, and the Fenton reaction. Moreover, different methods such as photodegradation, membrane filtration, adsorption, flocculation, reverse osmosis, irradiation, biosorption, biodegradation, ultrafiltration, nano-filtration, coagulation, sonolysis and sedimentation are ion exchange, trickling filtration, solvent extraction, electrocoagulation, activated sludge, and the use of microorganisms are used for the pollutant's removal (2,4,5). Methylene blue (MB) and Nile blue (NB) are thiazine cationic dyes. Methylene blue is used for biological staining as well as coloring paper, hair, cottons, and wools. The presence of MB in wastewater may result in a variety of health problems, including difficulty in breathing, vomiting, eye ignites, diarrhea, nausea, blindness, respiratory distress, and harmful environmental effects (6,7). Similarly, because of its tendency to bind to specific structures and tissues, NB is widely used in microscopy, microbiology, histology, and the textile sector. Furthermore, because NB dye can be used as an adsorbent to remove contaminants from water by binding to them, and it has been investigated for its prospective application in the removal of contaminants from wastewater. Furthermore, NB removes heavy metals such as lead and cadmium, organic contaminants such as dyes and pesticides, and radioactive compounds such as uranium. For the removal of these contaminants from wastewater, various types of nanomaterials have been widely used. For instance, Amr et al. have used silicotitanate for the removal of reactive blue and Congo red and the results showed good efficiency of the materials (8). Sujeong et al. have demonstrated that ZnO-200 nanoplates, after 3 h, exhibited a high sterilization performance of 96.95% (86.67% in a dark room) for Staphylococcus aureus and 95.82% (74.66% in a dark room) for Escherichia coli when irradiated with light (7). Saruchi et al. have also reported 95.7% adsorption efficiency for gum katira-silver nanoparticle-based Gk-cl-poly(AA)-AgNPs bio-nanocomposite (4). Sadighian et al. used GO-Au nanocomposite for the removal of MB and Methyl orange (MO) (9), Yaseen et al. employed CuO–SiO_2nanocomposite for the removal of crystal violet (CV) dye (10). Similarly, AgCl–ZnO was used by Gassimet al., for the removal of reactive black 5H (RB5H) (11). Tran et al. used Fe_3O_4/zeolite NaA nanocomposite for the removal of MB dye (6). Mohammed et al. used ZnO/Co_3O_4 nanomaterials for the removal of ciprofloxacin and azithromycin (12). Sadanand et al. have investigated that the under visible light irradiation, LBG-s-AgNPs@g-C_3N_4 NS (0.01 M) exhibited better photocatalytic performance i.e. ~100% RhB degradation and relative to MB degradation ~99% in 160 min (13). Ajel and Al-Nayili investigated Ag-WO_3/bent nanocomposites for the removal of umic acid (HA) (14). Areej et al. investigated NiCuMoO/rGO composite for the removal of MB with a photodegradation of 99.2% (15). Abinaya et al. utilized Ag_2MoO_4 nanocomposite in the removal of MB, Cr(VI), and CIP drug, and achieved 99.9%, 99%, and 99.8% removal performance in 10 min, respectively (16). Pourzare et al. utilized GO/Co_3O_4 nanocomposite in various dyes removal and achieved 98% removal for MB in 12 min, while 66% for Rhodamine B (RhB), and 45% for MO in 40 min (17). Sarika et al. used cowdung (CD) gamma-sterilized for the removal of triphenylmethane dyes crystal violet (CV), brilliant green (BG), and malachite green (MG) from an aqueous solution (18). Foroutan et al. reported the fabrication of CNT/MgO/$CuFe_2O_4$ composite and utilized in the removal of Methyl violet and NB dyes from wastewater (19). However, nanoparticles based on polymers have garnered a lot of attention in this field because of the impressive mechanical properties they exhibit after being modified with nanoscale additives. They are also magnetic, electrical, and optically active, and resistant to wear, flame, and heat. Several methods of fabricating polymer nanocomposites are addressed. Some examples of such techniques include: (1) in-situ polymerization, (2) solution-phase intercalation of

polymer, (3) direct-mixing of polymer and fillers, (4) intercalation in molten polymer, (5) template assisted synthesis, (6) sol–gel method, etc. Researchers are particularly interested in poly (vinyl alcohol) (PVA) due to its excellent film formation and physical qualities, high hydrophilicity, biocompatibility, and chemical resistance. The introduction of novel additives or nanomaterials can be used to modify or improve the characteristics of PVA (*20*). It has been demonstrated effectively that nanoscale addition results in improved features. By reducing inter-particle distance and boosting polymer matrix interaction strength, nanoscale additives with high surface area, high surface energy, and anisotropic geometry are used in new fields and contribute to improved spatial properties of conventionally lining polymers (*21*). Several researchers have employed polymer-based materials for wastewater treatment, such as, Zaheer et al. developed a CuO/PVA composite using a chemical reduction method. They observed that the composite materials removed 98% of the RhB dye, signifying its excellent removal performance (*22*). Soltaninejad et al. investigated that the PVA/ZnO/AgI/Chl photocatalyst exhibit exceptional performance for the degradation of MB, Congo red (CR), and 4-Chlorophenol (4-CP), with degradation performance of 95.5%, 92%, and 88%, respectively, as a result of varied parameter effects on the same photocatalyst (*23*). Malekkiani et al. used a sonication-based approach to investigate MWCNTs/ZnO/Chitosan nanomaterials. The results confirmed that the composite has a photocatalytic performance of 98.7% to 85% for MB dye (*24*). The PVA/CZnO$_2$ composite prepared by El-Shamy via solution casting method exhibited 98% performance toward MB dye degradation (*25*). Mottaleb et al. confirmed the successful synthesis of PAN/GO–ZnO composite through electrospinning process. The composite material degraded MB and Indigo carmine (IC) dyes with removal performance of 96% and 98%, respectively (*26*). Hussain et al. synthesized guar gum–polyacrylamide/erbium oxide nanocomposite (GG–PAAm/Er_2O_3NC) through crosslinking approach. The removal rate of NB over the nanocomposite was 97.3% (*27*). Abebe et al. prepared PVA-ZnO/Mn_2O_3 nanocomposite through sol–gel and self-propagation routes. The nanocomposite revealed a 74.35% removal performance for NB dye from wastewater (*28*). Likewise, Maijan et al. reported the fabrication of PVA-g-PAM/SiO_2@ZnO composite. The composite removed 96% of MB dye form wastewater (*29*). Moradi et al. employed Agar/GO/ZnO nanocomposite in the removal of MB and MO dyes and achieved about 88% and 91% removal, respectively (*3*).

According to the above literature, various catalysts behave differently toward the same dye, and the same dye can have varying attachment affinity for chemically distinct catalysts. The overall influence of these behaviors can be seen in the wastewater treatment process, either directly or indirectly. In order to extend our previous works (*10,30*) and modify the binary semiconductor materials, herein, we aimed to fabricate, characterize, and assess the adsorptive and photocatalytic the CuO–SiO_2/PVA based ternary nanocomposite samples. To the best of our understanding, the unique combination of CuO–SiO_2 with PVA polymer, employing sol–gel and in-situ polymerization methods, has not been reported before. Therefore, we employed a cost-effective and easy-to-handle approach to not only transfer the desirable properties of CuO–SiO_2 to the PVA matrix but also to modify the inorganic CuO–SiO_2-based material with a hydrophilic polymer. The effect of some experimental variables on the catalytic/photocatalytic activities of the CuO–SiO_2/PVA ternary nanocomposite toward the removal of two structurally different dyes, i.e. MB and NB dyes, was also studied. Kinetic studies, degradation, and removal performance of the composite material were compared with previously reported literature. The results concluded that our polymer composite showed appreciable activities compared to composite materials without polymer. Finally, the biological activities such as antioxidant and antileishmanial properties of the resultant composite were also investigated, aspects that had not been evaluated for the synthesized nanomaterials, adding some uniqueness to this study as well.

2. Experimental

2.1. Materials and methods

All of the chemicals used in the fabrication of nanocomposite and dye degradation studies were of analytical grade. The chemicals include copper nitrate trihydrate ($Cu(NO_3)_2{\cdot}3H_2O$), tetraethyl orthosilicate ($Si(OC_2H_5)_4$), glycerol ($C_3H_8O_3$), nitric acid (HNO_3), absolute ethanol (C_2H_5OH), Poly (vinyl alcohol) {PVA, $[CH_2CH]n$} (Sigma-Aldrich, St. Louis, MO, U.S.A.), and ammonia solution (30% NH_3, Merck), Nile blue (NB) and Methylene blue (MB) (purity, 99.99%) received from Exciton (Dayton, OH, U.S.A.) and used as such. Methylene blue and Nile blue have the molecular formulas $C_{16}H_{18}ClN_3S$ and $C_{20}H_20ClN_3O$, respectively, and their chemical structures are shown in Scheme 1.

2.2. Preparation of CuO–SiO_2/PVA polymer nanocomposite

The CuO–SiO_2/PVA ternary nanocomposite was synthesized through sol–gel process and in situ approach.

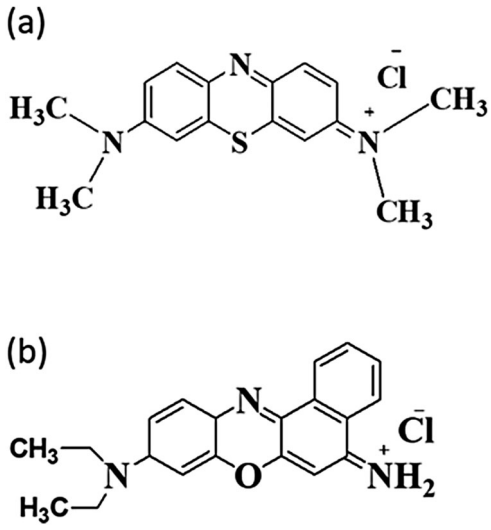

Scheme 1. Chemical structures of (a) Methylene blue (MB) and (b). Nile blue (NB).

In a typical experiment, $Cu(NO_3)_2{\cdot}3H_2O$: Glycerol: TEOS: PVA were mixed in a ratio of 8:2:3:4 i.e. 40 mL of copper nitrate trihydrate (1 M) solution was taken in a 200 mL beaker. Dropwise additions of 10 mL glycerol and 15 mL TEOS were then made to the mixture, which was then continuously stirred at room temperature while 30% HNO_3 was added to bring the reaction mixture's pH to 1.5. This process took roughly an hour. To bring the pH to 9, 30% ammonia was added after then. Following this, 20 mL of PVA solution was added dropwise while stirring continuously, and the mixture was then agitated for a further 3–4 h at 60°C. A slow-forming blue gel eventually turned black. The gel sample was then filtered out of the mixture and repeatedly washed with acetone and deionized water. The filtered gel was then submerged for 72 h in a solvent made of water and ethanol in a 1:1 ratio. To get a pure powder sample, the mixture was then filtered once more, dried at 90°C for 10 h, and finally calcined at 600°C for 3 h. The possible chemical reaction for the synthesis of nanocomposite is represented as;

$$Cu(NO_3)_2{\cdot}3H_2O + TEOS + glycerol + PVA + NH_4OH \rightarrow [Cu(TEOS)m(PVA)n] + 3H_2O + C_3H_8O_4 + (NH_4)_2SO_4$$

The stepwise synthesis procedure of the $CuO–SiO_2$/PVA polymer nanocomposite is presented in Scheme 2.

2.3. Characterization of the polymer nanocomposite

Several characterization methods, including UV-Visible, SEM, EDX, TEM, FTIR, DSC, and TGA, were used to learn more about the polymer nanocomposite ($CuO–SiO_2$/PVA). The powdered sample was dispersed in the solvent and then analyzed using a UV-Visible Spectrometer Lamda-25 (PerkinElmer) to determine its chemical composition. The polymer nanocomposites' external morphology was analyzed via SEM using a JSM-5910 JEOL scanning electron microscope. Using a JEM 2100F transmission electron microscopy (TEM)

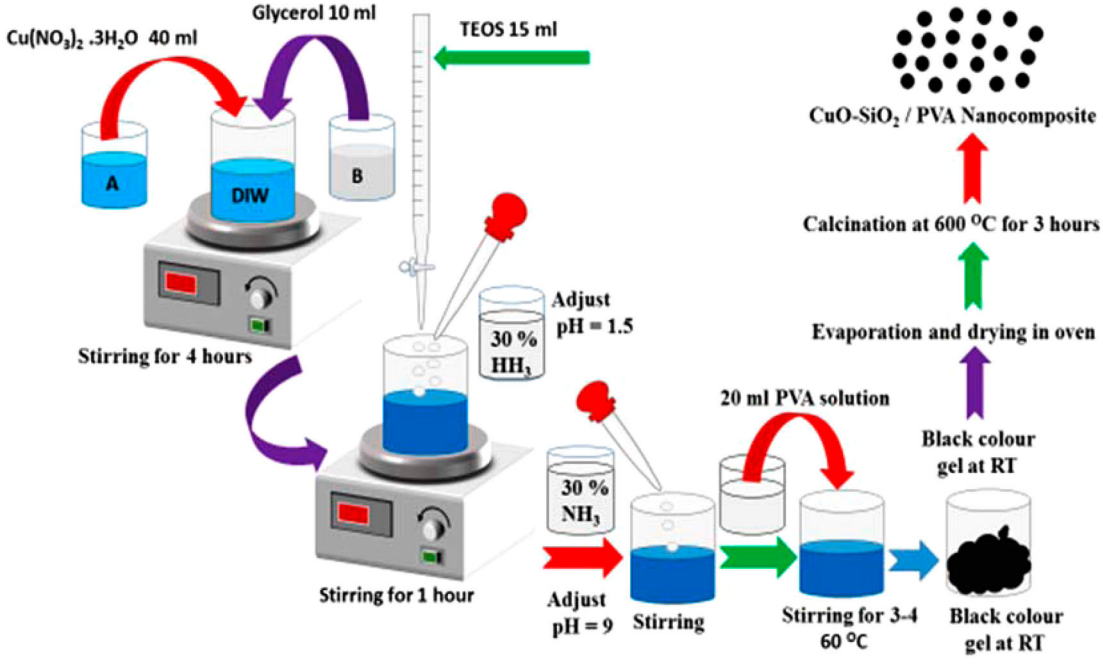

Scheme 2. Diagram illustrating the fabrication of a $CuO–SiO_2$/PVA polymer nanocomposite.

fitted with a 200 kV field emission gun, the samples' internal morphology was analyzed. The solid powder was further analyzed by FTIR (500-4000CM1) Nicolet 1S5 U.S.A. in the wave number ranges of 400 and 4000 cm^{-1}. Using a Shimadzu TG-50 (Japan) thermal analyzer, thermogravimetric analysis (TGA) was carried out between 25 and 1200 degrees Celsius at a rate of 5 degrees Celsius per minute in a nitrogen (N_2) atmosphere. In the meantime, differential scanning calorimetry (DSC) measurements were carried out with a DSC Q2000. Operating in a nitrogen atmosphere at a heating rate of 10°C/min within the temperature range of 25–1200°C, the apparatus (TA Instruments, Newcastle, Del., U.S.A.) and DTA (Differential Thermal Analysis) was utilized for DSC studies. The as-synthesized nanomaterials' thermal stabilities were investigated, and the transition temperatures and heat fluxes related with them were calculated.

2.4. Photocatalytic degradation of the dyes

The photocatalytic decomposition process was performed in a Pyrex beaker coated with aluminum foil to prevent light diffraction and concentrate on the reaction taking place inside the beaker. There is a 220 nm, 15 W UV-lamp installed in it. A magnetic stirring device was attached to a Pyrex glass beaker containing 100 mL of water containing 20 ppm of NB or MB solutions, and 0.1 g of the polymer nanocomposite was added. Nile blue (NB) and MB dyes were subjected to photodegradation in the dark and in the light with and without a CuO–SiO_2/PVA catalyst. To establish a dynamic adsorption–desorption equilibrium between the dye molecules and the catalyst surface, the dye solution was stirred in the dark for the first 30 min. At regular intervals, aliquots of roughly 10 mL were obtained and analyzed on a UV-Vis spectrophotometer by recording the absorbance at λ_{max}.

Degradation efficiency, kinetics, and removal efficiency were predicted via the following equations;

$$\text{Degradation efficiency (\%)} = \left(\frac{C_0 - C_t}{C_0}\right) \times 100 \quad (1)$$

$$\text{Removal efficiency } (Q_t) = \left(\frac{C_0 - C_t}{M}\right) \times V \quad (2)$$

$$\ln\left(\frac{C_t}{C_0}\right) = -k_{app}t \quad (3)$$

Q_t is the removal efficiency expressed in mg/g, V is the volume in Liters, M is the mass of the catalyst in gram, C_0 and C_t are the beginning and final concentrations (C_t is the concentration at time = t). Using Beer–Lambert law, the concentrations of the solutions were determined from the dye solutions' steady absorbance values. UV-Visible spectroscopy was used to compare the dye quantities before and after adsorption. The slope of plots of $\ln(C_t/C_o)$ vs reaction time (t) provides a good approximation of the apparent rate constant of the reaction (k_{app}). The second order kinetics equation was also applied to the data; however, it was found to be more in line with pseudo first order kinetics.

2.5. Biological application studies

Biological activities such as antioxidants and anti-leishmanial of the synthesized polymer nanocomposites were also investigated.

2.5.1. Antileishmanial activity

The synthesized polymer nanocomposite was tested for the antileishmanial activity. In this method, the polymer nanocomposite material was taken for screening of leishmanicidal activity (*30*). Leishmania tropica promastigotes, 10% FBS (Fetal Bovine Serum), 1% antibiotic (Miltefosine) and 1% Hepes(N-Hydroxyethylpiperazine-N'-ethanesulfonic acid) buffer were taken in the RPMI-1640 medium. In the Neubauer chamber, their numbers increased from 5 to 6 million cells per ml after their introduction into long phase. Nanocomposites were stored at various concentrations on a 96-well plate (1000, 500, and 250 g/ml) and tested in triplicate. Nanocomposites were disseminated in DMSO (dimethyl sulfoxide) (0.5%), serving as a negative control, and miltefosine, a potent leishmania inhibitor, was utilized as the locus drugs. One hundred microliters of full culture medium containing 104 cells per well and the screening nanocomposites at their essential, specified concentrations were used to seed the plate. The respective plates were incubated for 72 h at 25°C. Each nanocomposite's promastigotes that survived were tested using a colorimetric approach based on tetrazolium-dye (MTT). Each well of the 96-well plates was filled with 100 l of MTT dye diluted in PBS, and the plates were incubated at 37°C for another 3 h. Then, added 40 µl of DMSO as a stopping solution and had their ELISA Biotek plate reader read them at 570 nm. The percent inhibition of the polymer nanocomposite was found using the following formula:

$$\text{Percent Inhibition} = \frac{\text{mean OD of Sample} - \text{mean OD of Blank}}{\text{mean OD of positive control} - \text{mean OD of Blank}} \times 100 \quad (4)$$

2.5.2. Antioxidant activity

The antioxidant activity of the produced polymer nanocomposite was tested through the DPPH (1,1-diphenyl-2-picrylhydrazyl) technique. In this approach, several concentrations (i.e. 250, 500 and1000 µg/ml) of the nanocomposite were made. Ascorbic acid was used as a benchmark for quality control. One ml of each composite was combined with one ml of freshly prepared DPPH solution in methanol (0.12 mM), and then another four ml of methanol was added and the mixture was let to stand in the dark for 40 min. The composite's absorbance at 516 nm was then calculated. The composite IC50 values were also calculated and determined across a range of concentrations. The following equation was used to analyze the DPPH scavenger percentage.

$$\text{Radical Scavenging } \% = \frac{1 - A_a - A_b}{A_c} \times 100 \quad (5)$$

To clarify, 'A_a and A_b' denote the absorbance of the composite in the presence as well as the absence of DPPH, while 'A_c' denotes the absorbance of the reference solution.

3. Results and discussion

3.1. UV-visible and bandgap energy analysis

The UV-visible spectrometer (Lamda-25, PerkinElmer) was used to analyze the obtained CuO–SiO_2/PVA composite after dispersion in ethanol. As indicated in Figure 1, the analysis was carried out in the spectral range of 200–800 nm. Two distinct peaks are detected at 242 and 285 nm, as indicated in Figure 1(a). In the CuO–SiO_2/PVA composite, the wavelength peak at 242 nm corresponds to CuO–SiO_2, whereas the peak at 285 nm relates to PVA polymer.

The bandgap energy of the polymer nanocomposite is calculated via the following Tauc plot equation;

$$(\alpha h\upsilon)^{\gamma} = A(h\upsilon - Eg) \quad (6)$$

In this equation, α stands for absorption coefficient, h denotes Planck's constant, υ stands for photon frequency, A is the proportionality constant, E_g represents bandgap energy, and γ represents electronic transition (which could have the values 2, $^1/_2$, $^2/_3$, or $^1/_3$). Figure 1(b) displays the Tauc plot for a CuO–SiO_2/PVA composite. A straight line is generated by plotting $(ahv)^2$ versus (hv), which elucidates that the absorption edge results from an indirect allowed transition ($n = 1$ for a direct allowed transition). The optical bandgap (E_g) is shown by the point where the straight-line intercept. The composite has a direct bandgap energy of 2.7850 eV.

3.2. SEM, TEM and EDX analysis

Figure 2(a–e) displays the SEM, TEM, and EDX analyses of the produced polymer nanocomposite. Figure 2(a) reveals the SEM result, confirming that the CuO–SiO_2 is distributed uniformly across the polymer matrix, which possesses a certain porosity. In similar fashion, the TEM image in Figure 2(b) illustrates the presence of nano-sized CuO–SiO_2 particles in the polymeric matrix. In the present case, glycerol was used to improve the dispersion of the nanoparticles in the PVA matrix and to promote the formation of a porous structure of CuO–SiO_2/PVA composite. As during the drying process, the glycerol evaporates from the CuO–SiO_2/PVA composite leaving behind its spaces in the composite structure. These pores are said to provide additional surface area for catalytic/adsorptive removal of dyes from solution. These pores also contribute to the mechanical and

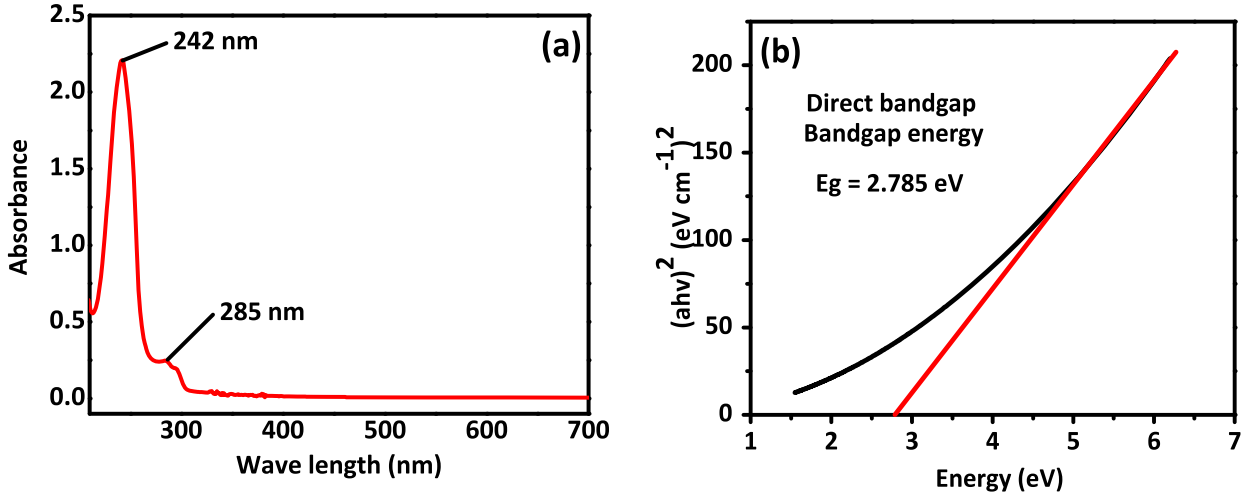

Figure 1. UV-visible spectrum (a), and bandgap energy (b), of CuO–SiO_2/PVA composite.

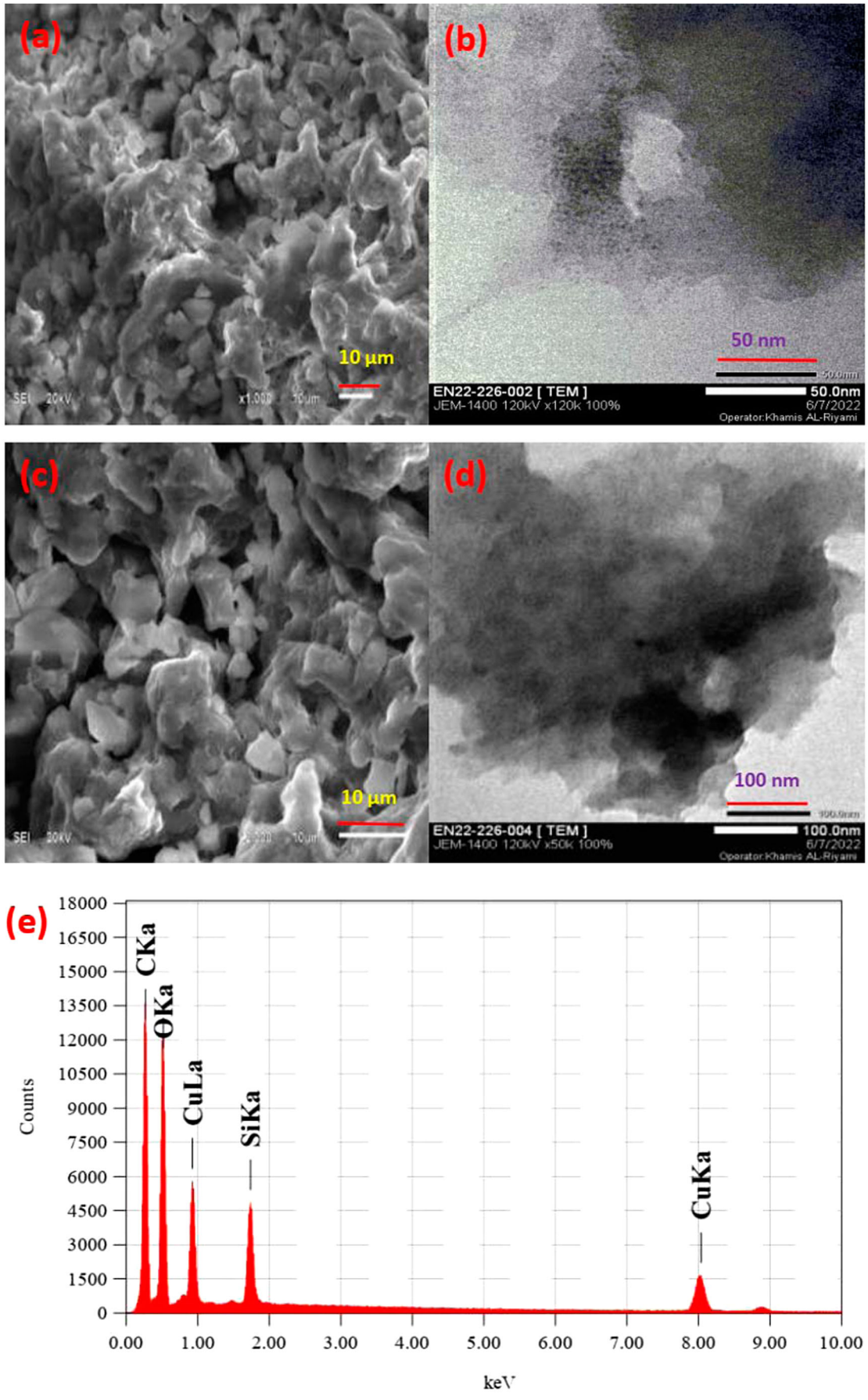

Figure 2. SEM images (a – before use) and (c – after the use), TEM image (b – before use) and (d – after the use), and (e) EDX spectrum of CuO–SiO_2/PVA composite.

thermal properties of the resulting CuO–SiO_2/PVA composites. Similarly, the Figure 2(c,d), indicates the SEM, TEM images of the synthesized nanomaterials after their use in dyes removal process. Further, the results shows that there observed no significant change in the structural morphology of the nanomaterials. It is important to note that used nanocomposite material were collected, washed, dried, and then subjected to SEM analysis. Moreover, the EDX analysis in Figure 2(e) carried out via the energy X-ray dispersive spectroscopy (EDX) clearly indicate that the corresponding peaks of C, O, Cu, and Si in the as-fabricated nanocomposite. Table 1 lists the identified elements along with their atomic and mass percentages.

3.3. FTIR analysis

FTIR investigations of the synthesized nanocomposites were performed using a U.S.-made FTIR (500–4000 cm^{-1}) Nicolet 1S5 while using the solid powder of the samples. Figure 3 shows the FTIR spectrum of the produced CuO–SiO_2/PVA composite. The corresponding Cu–O stretching vibration band arose at 444 cm^{-1}. The Si–O–Si bond's asymmetric and symmetric stretching vibrations are indicated by the peaks at 1043 and 832 cm^{-1}, respectively. The band at 1346 cm^{-1} is assigned to the CH_2 group of glycerol, while the bands at 1613 and 3341 cm^{-1} are associated with the bending and stretching vibrations of the OH groups.

Table 1. The elemental composition of CuO–SiO_2/PVA composite detected via the EDX analysis.

Elements	Mass %	Atomic %
C(K)	47.98	67.61
O (K)	17.76	18.78
Si (K)	13.31	8.02
Cu (K)	20.95	5.58

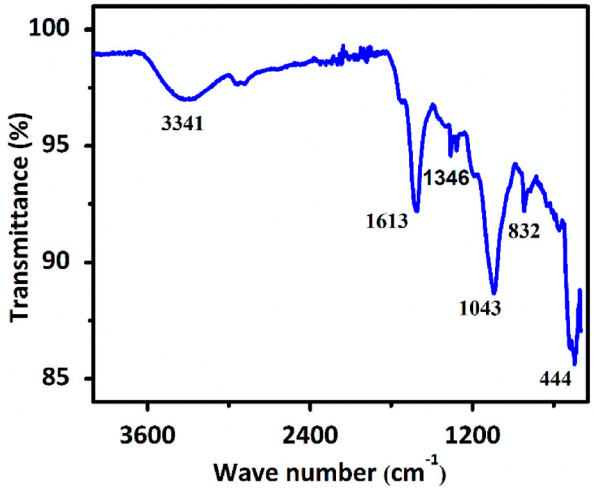

Figure 3. FTIR spectrum of the as-fabricated CuO–SiO_2/PVA polymer nanocomposite.

3.4. DSC and TGA analysis

Thermal analysis (TGA and DSC) of the as-synthesized nanocomposite was done to investigate the stability and to determine the temperature and heat flow associated with the composite transition as a function of time and temperature. The DSC and TGA spectrum of the CuO–SiO_2/PVA composite is shown in Figure 4. In Figure 4, the green line indicates the TGA curve with three distinct areas of temperature. At 172°C, the molecules of water over the surface of the composite evaporate, causing a 6% loss in initial mass. The second largest mass loss occurs at 293°C and is attributable to volatile components like glycerol; the final mass loss occurs at 659°C and is possibly attributable to degradation of the polymer (due to water evaporation from PVA) in the composite; and temperature above 659°C do not result in any mass loss %, suggesting that the composite is non-volatile. The blue line depicts the variation in heat flow; and the exothermic peaks arose at 96 and 708°C, while the endothermic peaks originate at 301 and 438°C.

3.5. Removal of NB and MB dyes via the catalytic and photocatalytic processes

The catalytic and photocatalytic removal of NB and MB dyes from aqueous solutions by CuO–SiO_2–PVA was studied to gain insight into the photocatalytic properties of the fabricated CuO–SiO_2–PVA composite. The UV-Visible setup was utilized for data analysis. The photocatalytic degradation process was carried out in a box made of wood with an aluminum foil-lined interior to concentrate the light over the reactor, emitting from a 15W UV-lamp. Photodegradation studies of NB and MB dyes (20 ppm) were carried out using CuO–SiO_2–PVA nanocomposites (0.1 g) in both light and dark, in the presence and absence of catalyst. Overall degradation was initiated by first stirring the dye-catalyst mixture for 30 min to equilibrate the dye molecules adsorbed on the surface of the photocatalyst. Aliquots of approximately 7 ml were withdrawn from the solution at regular time intervals by syringe, filtered and analyzed for absorbance at λ_{max} using a UV-Vis spectrophotometer. To determine the NB and MB dyes degradation rates, we used the following formula;

$$\text{Removal (\%)} = \left(\frac{A_0 - A_t}{m}\right) \times 100 \qquad (2A)$$

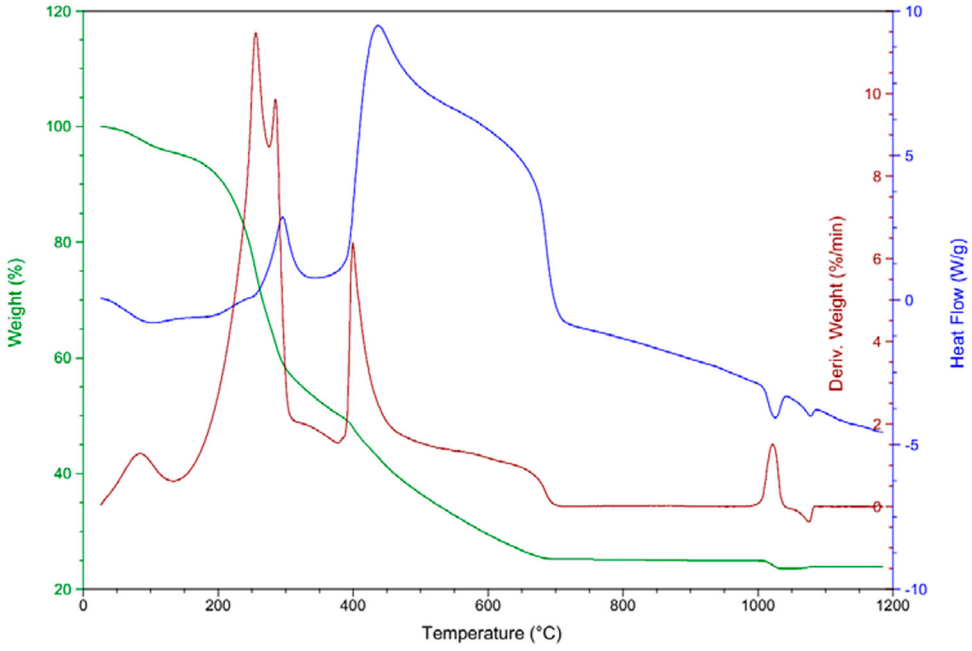

Figure 4. DSC, TGA spectra of the as-prepared CuO–SiO_2–PVA composite.

where 'A_0' represents the total absorbance at the start of the experiment and 'A_t' represents the final absorbance after certain period of time. Regarding the kinetics studies, the dye-removal data were tested through the following 1st order (Equation 3A), 2nd order (Equation 7), and the linear Elovich model (Equation 8).

$$\ln\left(\frac{A_t}{A_0}\right) = -kt \tag{3A}$$

$$\left(\frac{A_t}{A_0}\right) = -kt \tag{7}$$

$$q_t = \frac{1}{\beta}\ln(\alpha\beta) + \frac{1}{\beta}lnt \tag{8}$$

where in Equation (8), the terms β, α, and q_t reflect the adsorption rate (mg/g·min), the de-sorption constant (g/mg), and the quantity adsorbed at time 't' in (mg/g). The data was evaluated using the linear Elovich adsorption model by fitting the data directly in the origin using Equation (8). Similarly, 'C_o' stand for initial concentration at time $t = 0$, while 'Ct' denote the final concentration at $t = t$, of the NB and MB dyes solutions. The terms A_o and A_t denote absorbance at $t = 0$ and $t = t$, whereas, k_{app} represents the reaction apparent rate constant predicted from the slope of the plots of $\ln(A_t/A_o)$. These plots are depicted in Figures 5–9. Degradation of MB over time under light is illustrated by absorption plots against wavelength at regular time intervals. Figure 5(a) demonstrates that absorbance gradually decreased over time, confirming the efficient dyes degradation. Figure 5(b) shows the ratio of absorbance (A_t/A_0) vs. time, which allows us to monitor the MB dye's degradation in real time. The enhancement in % degradation over time is depicted in Figure 5(c), displaying a plot of decomposition % vs. time. The plot of the pseudo 1st order correlation for the degradation of MB is shown in Figure 5(d). Degradation data were used to determine whether the reaction follows a pseudo 1st order equation ($R^2 = 0.96612$). The value of the 1st order rate constant (K_1) is 0.00304 min^{-1}. As can be seen in Figure 5(e), which depicts the removal efficiency, this efficiency rises over time, peaking at around 720 min. Finally, Figure 5(f) illustrates the Elovich model in its linear form. The data were fitted to the linear equation, demonstrating a good fit with observed R^2 values of 0.96. This suggests an initial adsorption of the dye at the surface of the composite, followed by removal through the combined contribution of adsorption and photocatalysis. Furthermore, Figure 5(b) reveals that the data may not be well-suited for fitting in the second-order equation.

3.6. Removal of NB via catalytic and photocatalytic processes

Degradation of NB (20 ppm solution) under UV light and in the dark was investigated as well to learn more about the photocatalytic activity of CuO–SiO_2/PVA. The NB absorption peak intensity at $\lambda = 663$ nm is shown to decrease over time. There is a qualitative as well as quantitative transition in the degradation of NB with the catalyst CuO–SiO_2/PVA, as shown by spectroscopic data (Figures 6(a) and 7(a)). The results have also shown that

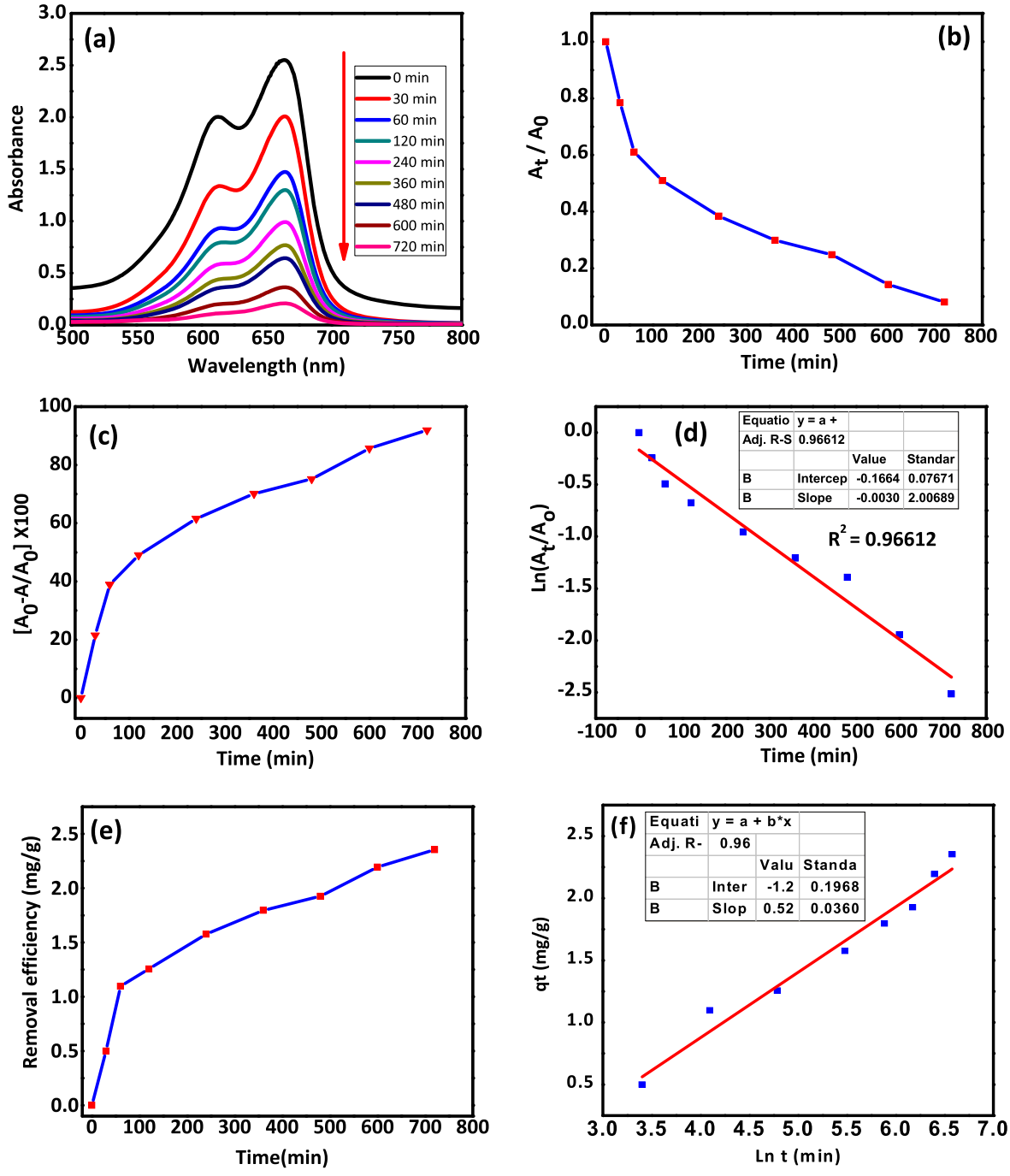

Figure 5. Summary of MB degradation in the presence of light: (a) changes in UV-visible absorption spectra at various times (b) absorbance rate (A_t/A_0) vs. elapsed time through second order approach, (c) percentage of decay in relation to time, (d) pseudo 1st order degradation kinetics plot, and (e) removal efficiency plot, and (f) linear Elovich model plot.

the NB intensity decreases with increasing irradiation time. This is mainly because NB molecules degrade during irradiation. Degradation of the NB dye with catalyst CuO–SiO_2/PVA was noticed by observing qualitative as well as quantitative changes in spectrum with time, which is further confirmed via the plot of percentage decomposition vs. time (Figures 6(b) and 7(b)), indicating the enhancement of degradation by means of the absorbance ratio (A_t/A_0) vs. time. The graphs of percentage degradation versus time in Figures 6(c) and 7(c) show that the degradation rate improves with time; these figures also show that the dye has been eliminated by 58% in 5 h in the dark and that 83% of NB could be removed by catalyst in the same length of time when exposed to light. The data show that the process of degradation follows pseudo 1st order kinetics with acceptable value of $R^2 = 0.95806$ in the presence of light and $R^2 = 0.97606$ in the absence of light, as depicted

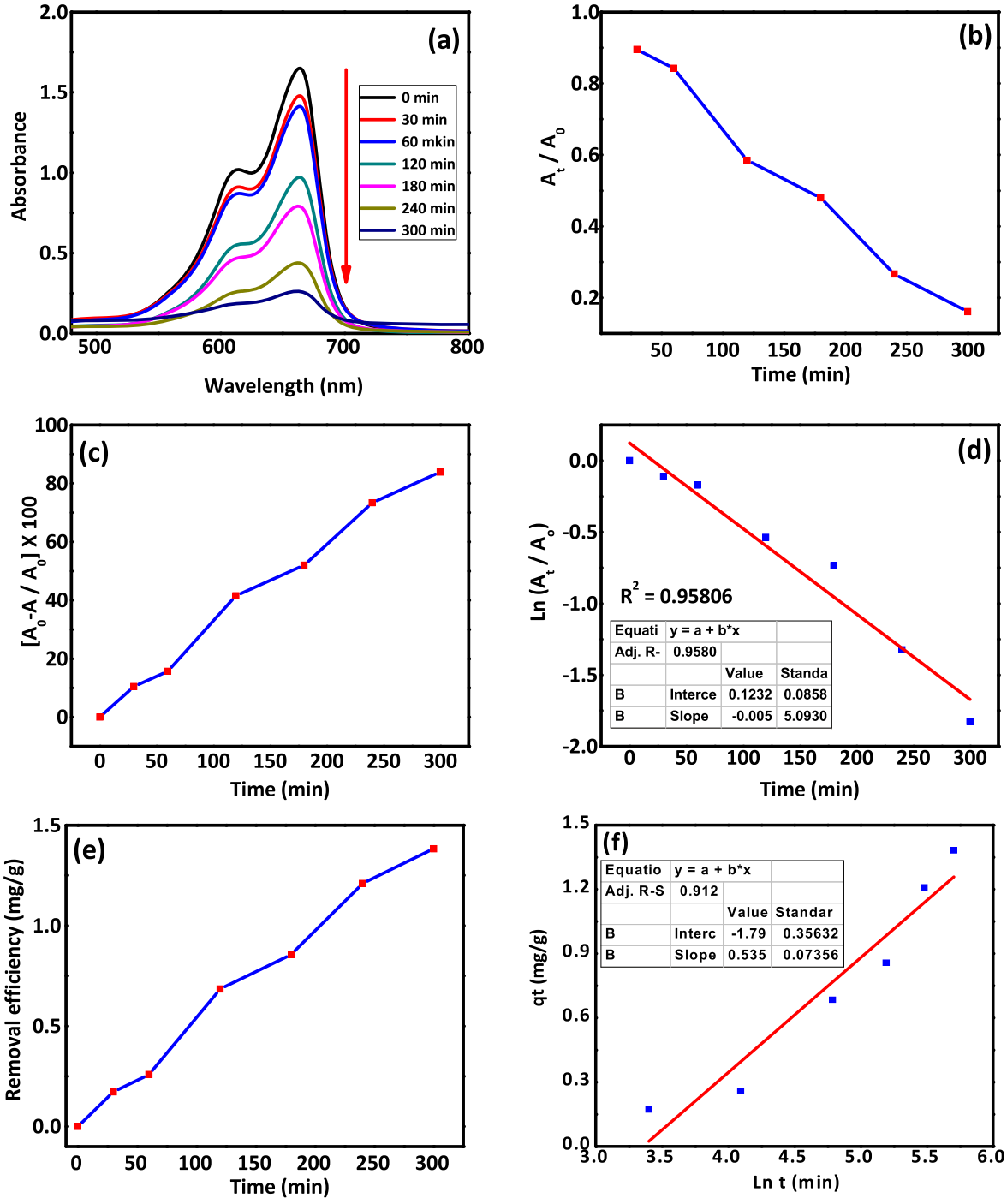

Figure 6. Brief summary of NB photodegradation in the presence of 0.1 g CuO–SiO_2/PVA catalyst: (a) changes in UV-visible absorption spectra at various times (b) absorbance rate (A_t/A_0) vs. elapsed time through second order approach, (c) percentage of decay in relation to time, (d) pseudo 1st order degradation kinetics plot, and (e) removal efficiency plot, and (f) linear Elovich model plot.

in Figures 6(d) and 7(d), respectively. Figures 6(e) and 7(e) show that the removal efficiency increases with time, reaching a peak at 300 and 361 min, respectively. These findings suggest that the CuO–SiO_2/PVA composite is effective at removing NB dye under both dark and light conditions, with the latter providing clearer evidence of its activity. The values of the rate constant (K_1) further corroborate this trend; the 1st order kinetics value for the removal of NB in the presence of light with no catalyst (i.e. 0.00304 min^{-1}), in the presence of catalyst (i.e. 0.00244 min^{-1}), and in the absence of light (i.e. 0.00598 min^{-1}) are shown in Table 2. Similarly, Figures 6(f) and 7(f) depict the Elovich model in its linear form. The data were fitted to the linear equation, showing a good fit with observed R^2 values of 0.912 and 0.900, respectively. The results strongly indicate that, initially,

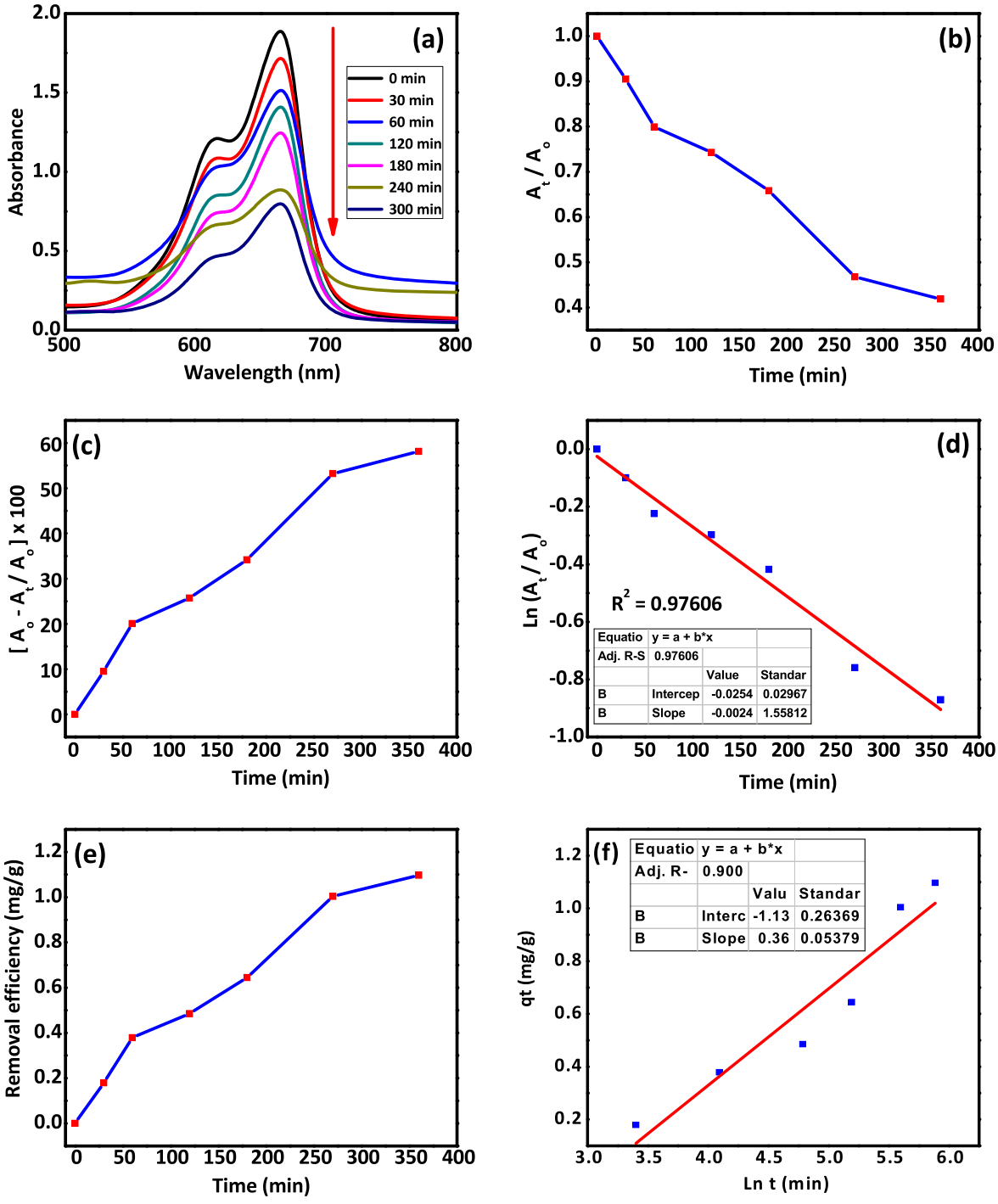

Figure 7. Summary of the NB degradation in darkness with the assist of 0.1 g CuO–SiO_2/PVA catalyst: (a) changes in UV-visible absorption spectra at various times (b) absorbance rate (A_t/A_0) vs. elapsed time through second order approach, (c) percentage of decay in relation to time, (d) pseudo 1st order degradation kinetics plot, and (e) removal efficiency plot, and (f) linear Elovich model plot.

dye molecules attach to the surface of the composite catalyst through physicochemical adsorption, consistent with the heterogeneous nature of the active sites, as evidenced by the adherence to the linear form of the Elovich model. The data was also tested with second order equation which was not followed accurately.

3.7. Removal of MB via catalytic and photocatalytic processes

The degradation of MB (20 ppm solution) under UV-light and the dark at different time intervals was studied to evaluate the photocatalytic activity of the CuO–SiO_2/PVA catalyst. It is found that the MB absorption peak

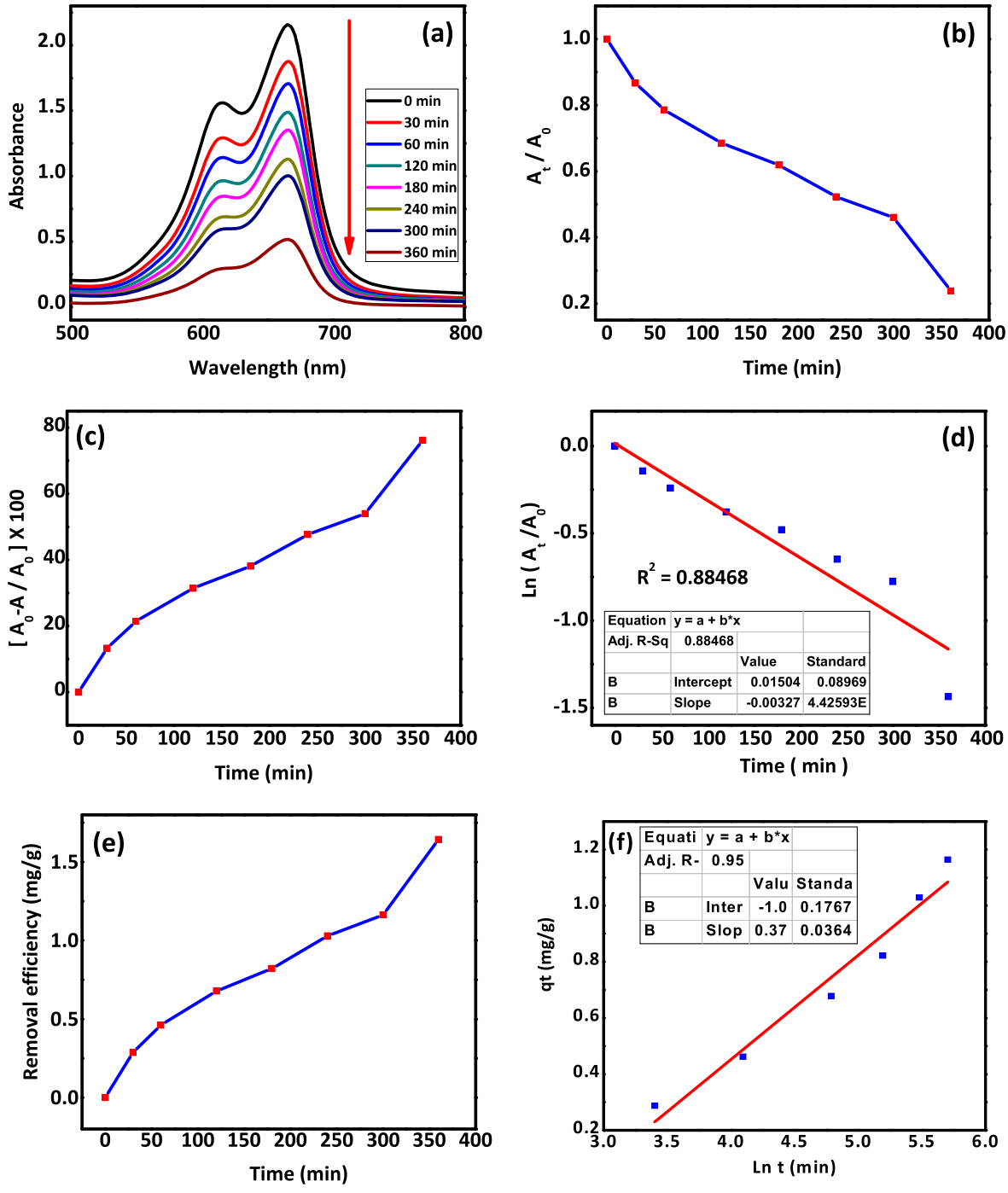

Figure 8. Summary of MB degradation with the assist of 0.1 g CuO–SiO_2/PVA catalyst under light: (a) changes in UV-visible absorption spectra at various times (b) absorbance rate (A_t/A_0) vs. elapsed time through second order approach, (c) percentage of decay in relation to time, (d) pseudo 1st order degradation kinetics plot, and (e) removal efficiency plot, and (f) linear Elovich model plot.

intensity at $\lambda = 663$ nm remarkably reduced with time. Figures 8(a) and 9(a) show the qualitative as well as quantitative changes observed via the UV-Visible spectrometer during the degradation of MB over CuO–SiO_2/PVA catalyst both in the presence and absence of light, respectively. Furthermore, the results revealed that the MB absorption intensity dropped as the irradiation time rose. This is due to MB molecules decomposition, which accelerates with the increase in irradiation time. Additionally, the plots in Figures 8(b) and 9(b) demonstrate an improvement in degradation with absorbance ratio (A_t/A_0) vs. time, indicating that MB dye is being degraded with the aid of CuO–SiO_2/PVA catalyst. The spectrum undergoes quantitative and qualitative changes throughout time, as indicated by plots of percent decomposition vs time. Plots of

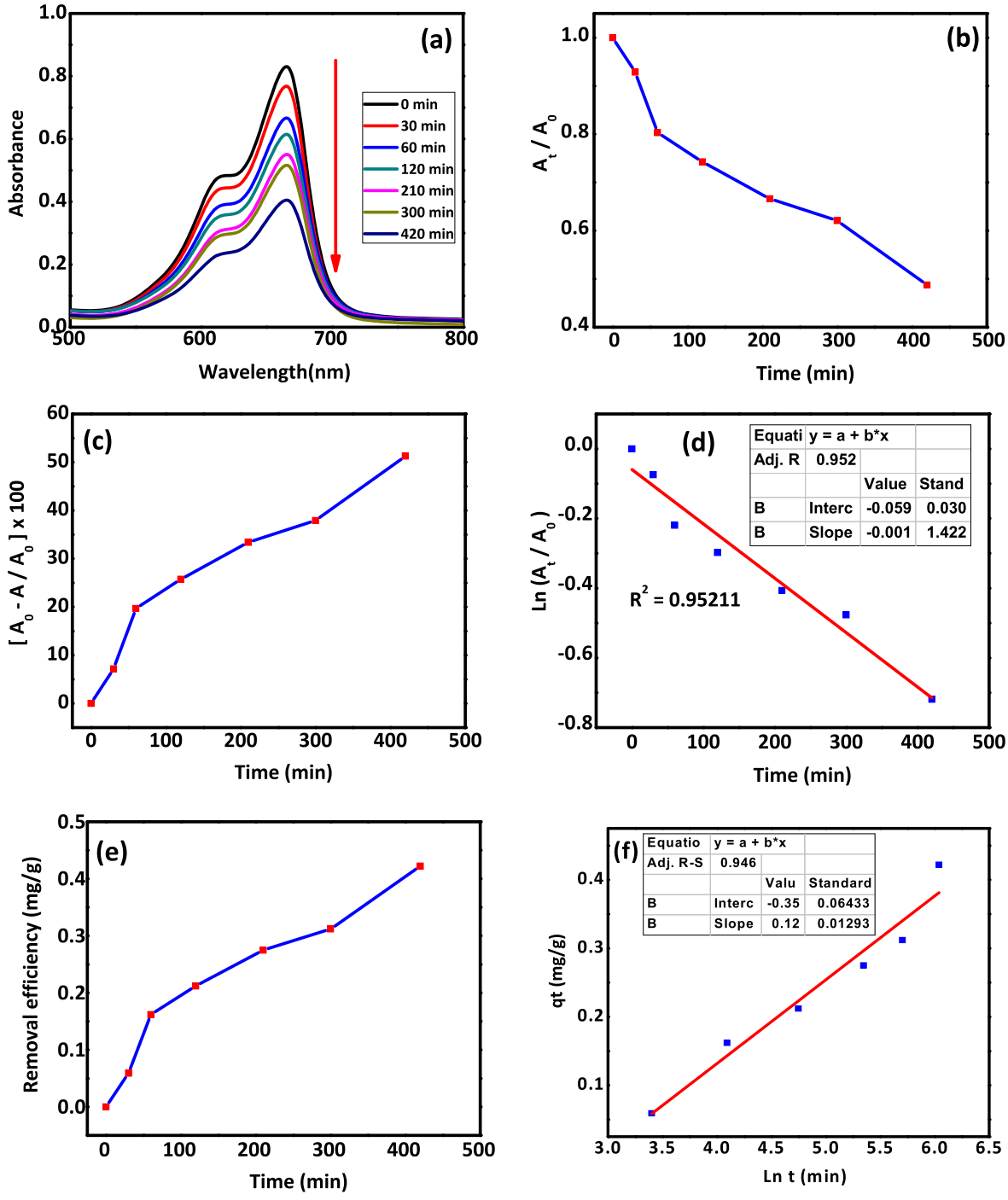

Figure 9. Summary of the MB degradation under dark conditions with the assist of 0.1 g CuO–SiO_2/PVA catalyst: (a) changes in UV-visible absorption spectra at various times (b) absorbance rate (A_t/A_0) vs. elapsed time through second order approach, (c) percentage of decay in relation to time, (d) pseudo 1st order degradation kinetics plot, and (e) removal efficiency plot, and (f) linear Elovich model plot.

Table 2. Degradation of NB via catalytic and photocatalytic processes, including 1st order rate constants and regression values.

Catalyst	Initial conc. of dye	Experimental time	Conditions	% removal	R^2 value for 1st Order Plot	1st order rate constant, k (min^{-1})
CuO–SiO_2/PVA (0.1 g)	NB 20 ppm	300 min	Light	83	0.958	5.74×10^{-3}
CuO–SiO_2/PVA (0.1 g)	NB 20 ppm	300 min	Dark	58	0.976	2.44×10^{-3}

percent degradation vs time in Figures 8(c) and 9(c) illustrate that percentage degradation rises with time. These findings also show that 51% of the dye is removed in 7 h under the dark, while 76% of the MB is catalytically removed under the light in 6 h. The pseudo 1st order correlations for the decomposition process are shown in Figures 8(d) and 9(d), and the data suggest pseudo 1st order kinetics with reasonable value of $R^2 = 0.88468$ in light and $R^2 = 0.95211$ in the absence of light. Figures 8 (e) and 9(e) show that dye removal performance improves over time, peaking at 360 and 420 min, respectively. These results indicate that the CuO–SiO_2/PVA composite demonstrates outstanding MB dye removal efficiency in both dark and light conditions, but with increased activity in the presence of light in contrast to performance in the dark. The value of the rate constant (K_1) further confirms this pattern. The 1st order kinetic constant values for MB removal are determined to be 0.00304, 0.00156, and 0.00327 min^{-1} for MB removal in the absence of a catalyst, in the presence of a catalyst under a dark environment, and in the presence of light, respectively (Table 3). In addition, the Figures 8(f) and 9(f) indicate the plots corresponding to the linear version of Elovich model; it can be seen that the dye-removal data in this case is also well-fitted to this kinetics model as evident from the R^2 values of 0.95 and 0.94 respectively. All such findings suggest a crucial initial step where dye molecules undergo attachment to the surface of the composite catalyst through a process of physicochemical adsorption. This observation aligns well with the heterogeneous nature of the active sites, as evident from the conformity to the linear form of the Elovich model. Furthermore, the dataset underwent testing using the second-order equation, but the fit was not accurate. This implies that the primary mechanism involves physicochemical interactions at the active sites, with limited adherence to the second-order kinetics model.

3.8. Comparative studies on the effectiveness of CuO–SiO_2/PVA composite toward the removal of NB and MB dyes under similar conditions

Table 4 shows a brief comparison of the dye removal efficiency of CuO–SiO_2/PVA catalyst with some of the previously reported nanocomposite materials and dyes. The efficiency of different nanocomposites in removing pollutants can vary depending on the specific pollutant being targeted or the particular nanomaterial being used. Various factors, such as chemical structures and reactivity of the catalyst toward pollutants, as well as variations in light, pH, and the amount of catalyst and pollutant present, can affect the pollutant removal process. In the present study, it was observed that CuO–SiO_2/PVA polymer nanocomposites can remove Nile Blue (NB) more effectively compared to Methylene Blue (MB); this difference may be due to variations in their chemical structure, charge, molecular mass, and pH sensitivity. In general, the chemical structures of both dyes are almost similar with some minor differences. Methylene Blue (MB) has a single methyl group attached, whereas Nile Blue (NB) has two methyl groups attached to the thiazine rings (SCN) at positions 6 and 7. In addition, Nile blue (NB) has a phenyl group (C_6H_5) on the thiazine ring and methylene blue has a dimethylamino group ($(CH_3)_2N$) at the 3-position. In addition, Nile blue (NB) has a Cl^- ion as a counter-ion, whereas methylene blue has a Cl^- ion plus an additional methyl group attached to one of the N atoms of the dimethylamino group $(CH_3)_2N$. Based on molecular weight, Nile Blue has a molecular weight of 364.89 g/mol, which is higher than methylene blue with a molecular weight of 319.85 g/mol. The interaction of Nile blue (NB) and methylene blue (MB) with UV and visible light depends on various factors such as wavelength, time of exposure to light, light intensity, solvent, and dye concentration. Furthermore, methylene blue (MB) is generally reported to be more stable than Nile blue (NB) under UV and visible light at neutral pH, although the stability of these dyes may vary depending on specific experimental conditions and other conditions. This is another possible reason for the higher removal rate of Nile Blue (NB) dye compared to methylene blue under similar experimental conditions used in this study. Likewise, the pH level of the medium plays a significant role in the electrical charge of the CuO–SiO_2/PVA nanocomposite. In acidic media, CuO exists in the form of Cu^+ ions, providing a positive charge to the composite. However, in basic media CuO forms $Cu(OH)_2$ and the

Table 3. First order rate constants and regression coefficients for catalytic and photocatalytic degradation of MB.

Catalyst/Amount	Initial conc. of dye	Experimental time	Conditions	% Removal	R^2 value for 1st Order Plot	1st order rate constant, k (min^{-1})
–	MB 20 ppm	720 min	Light	91	0.971	2.00×10^{-3}
CuO–SiO_2/PVA (0.1 g)	MB 20 ppm	420 min	Dark	51	0.952	1.56×10^{-3}
CuO–SiO_2/PVA (0.1 g)	MB 20 ppm	360 min	Light	76	0.884	3.27×10^{-3}

Table 4. A comparison of the removal effectiveness of CuO–SiO_2/PVA catalyst with previously reported materials.

S. No	Catalyst/Amount	Initial conc. of dye	Experimental time	Conditions	% removal	R^2 value for 1st Order Plot	1st order rate constant, k (min^{-1})	References
1	CuO–SiO_2/PVA (0.1 g)	NB 20 ppm	300 min	UV Light	83	0.958	5.74×10^{-3}	Present Work
2	CuO–SiO_2/PVA (0.1 g)	NB 20 ppm	300 min	Dark	58	0.976	2.44×10^{-3}	Present Work
3	–	MB 20 ppm	720 min	UV Light	91	0.971	2.00×10^{-3}	Present Work
4	CuO–SiO_2/PVA (0.1 g)	MB 20 ppm	420 min	Dark	51	0.952	1.56×10^{-3}	Present Work
5	CuO–SiO_2/PVA (0.1 g)	MB 20 ppm	360 min	UV Light	76	0.884	3.27×10^{-3}	Present Work
6	CuO–SiO_2 (0.1 g)	NB & RhB 20 ppm	300 min	UV light	90 85		8.60×10^{-3} 7.50×10^{-3}	(30)
7	CuO–SiO_2 (0.1 g)	NB & RhB 20 ppm	360 min	dark	90 85	0.958 0.983	2.00×10^{-3} 5.90×10^{-3}	(30)
8	Mn/BiOCl and Mn/NiO (0.7 g)	NB 20 ppm	480 min	Visible–light	98.4 98.7	–	3.90×10^{-2} 3.60×10^{-1}	(31)
9	CuO–SiO_2 (0.1 g)	CV 20 ppm		Visible Light	70	0.931	3.27×10^{-3}	(10)
10	CuO/PVA (0.00015 g)	RhB –	75 s	–	98	–	–	(22)
11	CuO–Mg–PVA (0.2 g)	MB 20ppm	180 min	UV Light	95.71	–	–	(32)
12	PVA/ZnO/AgI/ChI (0.1 g)	MB 10 ppm	60 min	Visible–light	95.5	–	–	(23)
13	MWCNTs/ZnO/ Chitosan (0.025 g)	MB 5 ppm	20 min	UV Light	98.76	–	–	(24)
14	PVA/$CZnO_2$ (0.04 g)	MB 2000 ppm	60 min	UV Light	98	–	–	(25)
15	poly(Py-co-Th)//ZnO (20 mg)	MB –	420 min	Sun Light	95.3	–	–	(33)
16	PAN/GO-ZnO –	MB & IC 50mL	70 min & 27 min	Visible Light	96 & 98	–	–	(26)

presence of (OH^-) or other Cu species gives the composite a negative charge. Similarly, SiO_2 is electrically neutral but is an insulator with charged functional groups such as silanol (Si–OH) and siloxane groups (Si–O–Si) on its surface. In acidic media, the silanol groups (Si–OH) are protonated, creating a positive charge in the composite. On the other hand, basic media can deprotonate the silanol groups (Si–OH), creating a negative charge in the composite. When the pH of the medium is acidic, PVA is protonated, creating a positive charge on the functional groups of the polymer chains (such as $–NH_3^+$ or –COOH groups), making the entire PVA positively charged. However, in basic media, deprotonation occurs, resulting in negative charges on functional groups such as $–COO^-$ and –OH on the polymer chains, giving PVA an overall negative charge. At neutral pH, PVA can enter a zwitterionic state at the pK_a of the polymer, resulting in an overall neutrality of PVA. In acidic media, both NB and MB exist in protonated form and carry a positive charge. However, in basic media, quaternary ammonium ions ($N^+(CH_3)_3$) and N atoms lose protons and become zero charge. Under neutral conditions, their presence depends on specific conditions and concentrations and can exist in both protonated and unprotonated forms. When NB and MB are dissolved in water in the presence of CuO–SiO_2/PVA, they interact with the composite materials and get adsorbed. NB has high adsorptive capacity due to possible intermolecular interactions such as van der Waals and hydrogen bonding, whereas MB has low adsorptivity due to bulky groups on the nitrogen, resulting in low attractive and adsorptive forces. Become. As a result, the MB has a lower removal efficiency compared to the He-NB dye. The active sites on the surface of CuO–SiO_2/PVA may also play an important role in the present case; these active sites may include hydroxyl ($^-$OH) groups, which can act as hydrogen bond donors, as well as carboxyl (–COOH) and amino ($–NH_2$) groups, which can act as electron donors and acceptors in surface adsorption reactions. The attachment of Nile blue (NB) and Methylene blue (MB) to the active sites on the surface of CuO–SiO_2/PVA could occur through a combination of physical adsorption and chemical bonding interactions. Physical adsorption involves weak Van der Waals forces, hydrogen bonding and electrostatic interactions, while chemical bonding interactions involve covalent bonds or

coordination bonds between the dye molecules and the active sites on the surface of the composite. Consequently, it is important to consider the ionic nature of these dyes when studying their behavior in aqueous solutions. As this characteristic can directly affect the dye's solubility, stability, and its interaction with other molecules near and/or on the surface of the material. The possible mechanism for the attachment and removing the two dyes MB and NB with CuO–SiO_2/PVA is shown in Scheme 3. The dye reaches the surface of the catalyst first. There, they bind with the catalyst surface through intermolecular forces (such as hydrogen bonding and London dispersion forces) and establish a dynamic equilibrium between the dye molecules on the catalyst surface. These dyes are removed from wastewater in the presence or absence of light. This removes these harmful contaminants from polluted water.

In addition to the above-mentioned factors, the efficiency of adsorptive and photo-assisted dye removal processes is notably influenced by factors such as dye concentration, catalyst amount, medium pH, and removal temperature. These parameters were systematically investigated in our previous studies to understand their impact on the dye-removal process (*34*,*35*). The influence of most of the aforementioned parameters on the dye removal process can be estimated based on existing literature easily. The expected outcomes of the pH variation reflect that the pH of the solution can considerably influence the surface charge of the CuO–SiO_2/PVA nanocomposite as well as the

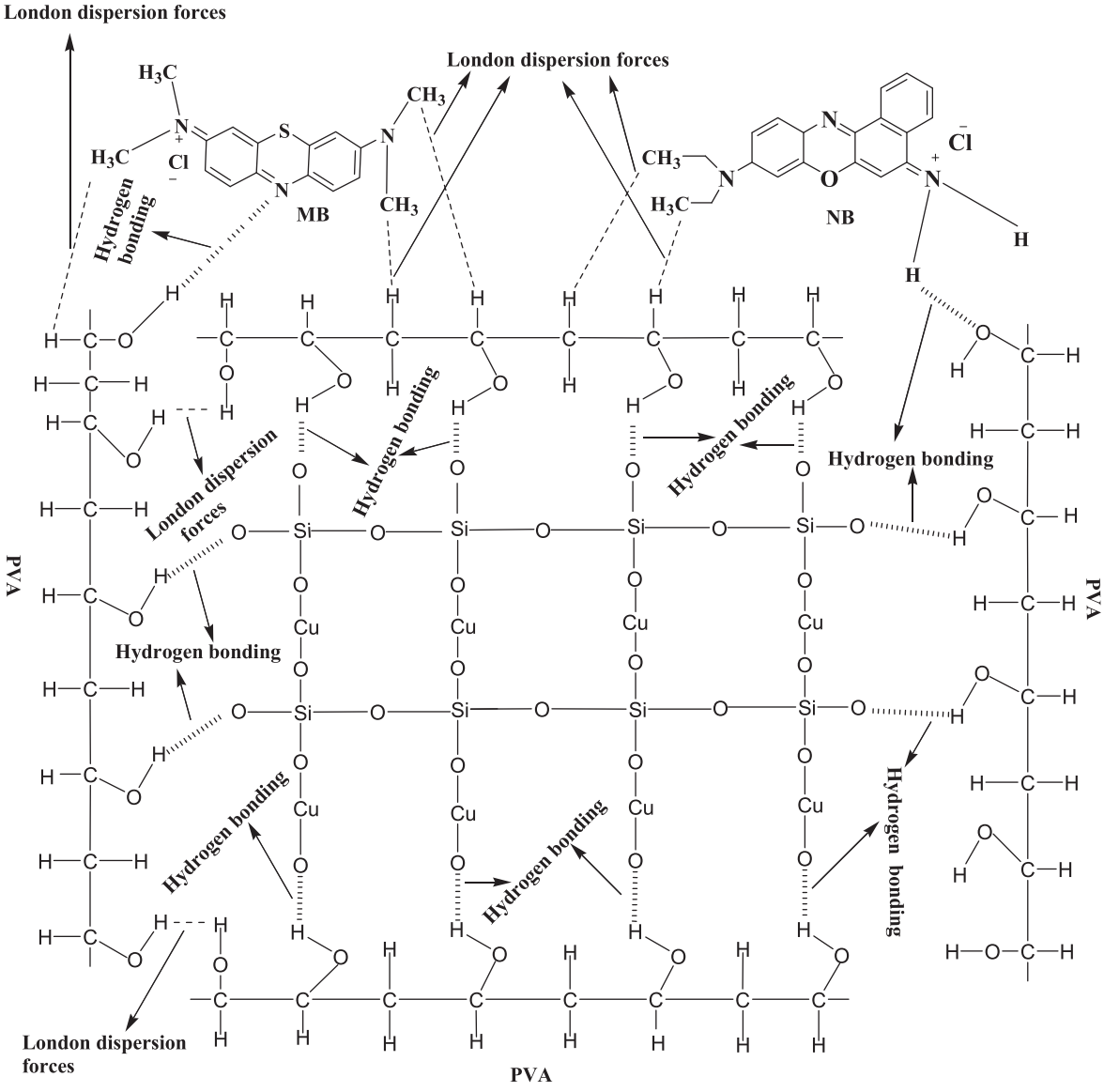

Scheme 3. Schematic representation of the mechanism for the MB and NB dyes removal using CuO–SiO_2/PVA polymer nanocomposite.

ionization state of the dye molecules. As discussed above, at different pH level the dyes will behave differently to interact with the nanocomposites and will affect the dye-removal effectiveness of the material. Similarly, various factors such as the material's adsorption and photocatalysis efficiency, thermodynamic saturation of the catalyst's active sites, reaction kinetics, photodegradation products, and the quality and quantity of penetrating light can influence the pollutant-removal process in aqueous media. Elevated dye concentrations initially boost photodegradation by exposing more molecules to light. However, beyond a certain point, photodegradation diminishes due to increased absorption at the sample's top or edges, limiting photon reach to the entire sample. Temperature also impacts photodegradation; higher temperatures can accelerate the process, but excessive heat may compromise catalyst stability, thereby affecting its efficiency. The catalyst amount affects the rate of dye degradation by providing active sites for dye attachment. Consequently, a higher catalyst amount generally means more active sites; however, excessive nanocomposite amounts can lead to agglomeration, light scattering, and reduced photodegradation effectiveness. The quality and intensity of irradiation also play a crucial role in the process. Therefore, it is recommended to consider a well-balanced combination of all experimental variables to achieve desirable and fruitful outcomes.

3.9. Performance stability and recyclability of the catalyst

The performance stability and reusability of the CuO–SiO_2/PVA polymer nanocomposite were also studied. These properties were evaluated through recycling tests for the removal of both NB and MB dyes, as shown in Figure 10. In a typical experiment, the nanocomposite used in each cycle was recovered, cleaned, and dried in an oven at 90°C for about half an hour before being reused. A similar process was employed for dye removal, with a fixed irradiation time of 6 h for each dye. The percentage removal efficiency was calculated and plotted against the number of cycles. Over four continuous cycles, it was observed that the catalyst's efficiency slightly reduced. This variation in efficiency may be attributed to a small amount of material wastage and/or a minor change to the catalyst's surface. The satisfactory recycling efficiency reflects the good performance stability of the nanocomposite in the current experimental setup. In addition, after using the nanocomposite material in the dye removal process, the collected materials were washed, dried, and then subjected to structural and morphological tests. As shown in Figure 2(c,d), there was no significant change observed in the structural morphology of the nanomaterials. These results further support the stability of the fabricated CuO–SiO_2/PVA composite.

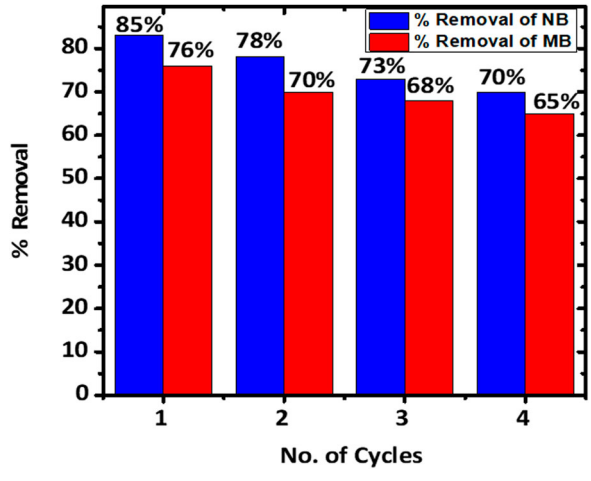

Figure 10. Recycling ability of CuO–SiO_2/PVA composite toward NB and MB dye removal. The concentration of dye 20 mg L^{-1}, the amount of catalyst 0.1 g, temperature 25°C, and time 6 h.

3.10. Biological activities of the CuO–SiO_2/PVA composite

The antioxidant activity of the CuO–SiO_2/PVA composite has been evaluated using the technique known as DPPH, and the results are shown in Figure 11(a) and Table 5. In this technique, ascorbic acid is chosen as a typical positive control. It has been found that as the concentration increases, the antioxidant activity also enhances (*10,36*). Figure 11(a) demonstrates the way the antioxidant activity of the catalyst changes with solution concentration. Antioxidant activity with different concentrations of solution is in the order of 1000 g/mL >500 g/mL >250 g/mL, demonstrating that the higher the concentration, the stronger the antioxidant activity. Similarly, the antileishmanial activity of the catalyst was tested, and the results are shown in Table 5(b). For this purpose, Miltefosine was used as a reference drug and DMSO as a negative control. It is important to mention here that the choice of DMSO as a negative control in the antileishmanial method and its potential interactions with the catalyst are crucial for confirming transparency and reliability in such investigations. Generally, DMSO is used as negative control solvent due to its wide use in biological assays, good ability to disperse the heterogeneous catalyst/testing material, and its inertness. This solvent is generally considered inert, meaning it does not participate significantly in chemical reactions. It is also expected to have minimal impact on the antileishmanial activity and this can allow the researchers to isolate the effects of the

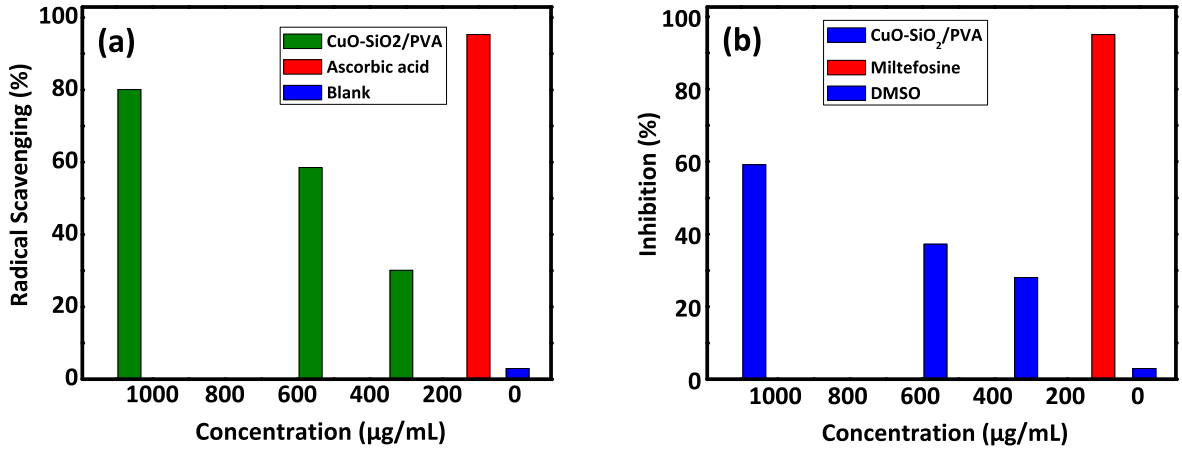

Figure 11. (a) Antioxidant activities, and (b) Antileishmanial activities of the CuO–SiO_2/PVA composite.

Table 5. Summary of the antioxidant and antileishmanial activities of the CuO–SiO_2/PVA composite.

Sample	Concentration (µg/mL)	% Activity	IC_{50}µg/mL
Antioxidant activity			
Standard (Ascorbic Acid)	100	95.27	410.74
CuO–SiO_2/PVA	250	80.11	
-do-	500	58.48	
-do-	1000	30.09	
Antileishmanial activity			
Standard (Miltefosine)	100	95.05	406.80
CuO–SiO_2/PVA	250	77.95	
-do-	500	56.78	
-do-	1000	34.61	

catalyst only, hence, it is a better choice to use as a negative control. Although DMSO is generally considered inert, however, there may still be some minor potential interactions between DMSO and the CuO–SiO_2/PVA composite due to the presence of organic moiety (PVA). Due to this possible interaction the CuO–SiO_2/PVA composite may undergo changes in its inherent properties when DMSO-Composite interactions are stronger, and thereby the antileishmanial activities of the composite may be affected under such conditions. Previous work (*10*) reveals that the antileishmanial activity fluctuates with concentration, i.e. the antileishmanial activity is higher at higher concentrations of the catalyst and vice versa. Figure 11(b) indicates that as the solution concentration increases, the antileishmanial activity of the catalyst also increases. The antileishmanial activity of the catalyst at different concentrations is in the order of 1000 g/mL > 500 g/mL > 250 g/mL. The increase in biological activities such as antioxidant and antileishmanial effects with an increase in the concentration of CuO–SiO_2/PVA nanomaterials may be attributed to some vital factors, including increased scavenging of reactive species, a larger surface area, and the availability of a greater number of active sites on the composite surface. Similarly, improved bioavailability, concentration-dependent biological responses, and synergistic effects, optimal conditions for interaction, and enhanced stability and durability of the composite material may also contribute. Most of these factors contribute to the enhancement of the biological activities of the nanomaterials with an increase in the concentration of the nanocomposite.

4. Conclusion

Herein, ternary nanocomposite based on CuO–SiO_2/PVA has successfully been fabricated via a low cost sol–gel based in-situ approach while utilizing $Cu(NO_3)_2{\cdot}3H_2O$:Glycerol:TEOS:PVA in a ratio of 8:2:3:4. The fabricated composites were characterized by UV-Visible, FTIR, SEM, TEM, EDX, TGA and DSC techniques to obtain information on structure, morphology, elemental composition, crystallinity, thermal stability and thermal change. Based on the results obtained here and in the light of available literature, it was found that the composite shows appreciable surface, morphological, and thermal characteristics. The catalytic and photocatalytic performance of CuO–SiO_2/PVA polymer nanocomposite was assessed toward the removal of two structurally related dye, such as Nile blue and Methylene blue, from water under different experimental conditions. Moreover, it was also proved experimentally that the prepared polymer nanocomposite could remove the NB (85%) easily and rapidly in comparison to the MB (76%); and this is accredited to the variation in the chemical structures/nature, charge, molecular mass, and pH sensitivity of both dyes. The formation of active sites over the surface of catalyst may also be advantageous for the effective removal of ionic or inorganic contaminants from water via electrostatic interactions. According to the kinetic analysis, the process of dye removal follows a pseudo 1st order kinetics mechanism. The active sites on the surface of CuO–SiO_2/PVA

may also play an important role in the present case; these active sites may include hydroxyl (–OH) groups, which can act as hydrogen bond donors, as well as carboxyl (–COOH) and amino ($–NH_2$) groups, which can act as electron donors and acceptors in surface adsorption reactions. The attachment of NB and MB to the active sites on the surface of $CuO–SiO_2$/PVA could occur through a combination of physical adsorption and chemical bonding interactions. Moreover, the biological activities like (antioxidant and antileishmanial) were also evaluated for the synthesized nanocomposite. The enhanced biological activities of $CuO–SiO_2$/PVA nanomaterials with increasing concentration can be attributed to factors such as increased scavenging of reactive species, a larger surface area providing more active sites, improved bioavailability, concentration-dependent biological responses, synergistic effects, optimal interaction conditions, and enhanced stability and durability of the composite material. Based on the overall results, it is suggested that this ternary nanocomposite has better potential to remove contaminants and microorganisms from wastewater and improve wastewater quality.

Acknowledgements

The authors are grateful to Abdul Wali Khan University Mardan, Pakistan, and Prince Sultan University, Riyadh, Saudi Arabia for the overall support during this work. Authors would like to thank Prince Sultan University for paying the APC. All authors have contributed to this study at different stages. Muhammad Yaseen and Abbas Khan: study design, method design, analytical protocol design, writing, reviewing, and editing. Muhammad Humayun and Abbas Khan: experimental assistant, discussion during writing, and reviewing. Shaista Bibi and Sajjad Ahmad: experimental assistant, biological activities, and data analysis. Saima Farooq, Abbas Khan, Muhammad Humayun, and Mohamed Bououdina: reviewing, and editing. All authors read and approved the final version of this manuscript.

Disclosure statement

No potential conflict of interest was reported by the author(s).

Funding

We declare that no special funds, grants, or other support were received during the preparation of this manuscript; however, the Department of Chemistry at Abdul Wali Khan University Mardan provided the basic chemicals and working space during this study.

ORCID

Abbas Khan http://orcid.org/0000-0002-2882-8761
Muhammad Humayun http://orcid.org/0000-0003-3504-3935

References

[1] Panaday, S.; Makhado, E.; Kim, S.; Kang, M. Recent Developments of Polysaccharide Based Superabsorbent Nanocomposite for Organic Dye Contamination Removal from Wastewater – a Review. *Environ. Res.* **2023,** *217*, 114909. doi:10.1016/j.envres.2022.114909.

[2] Yaseen, M.; Khan, A.; Humayun, M.; Farooq, S.; Shah, N.; Bibi, S.; Khattak, Z.A.; Rehman, A.U.; Ahmad, S.; Ahmad, S.M. Facile Synthesis of Fe_3O_4-SiO_2 Nanocomposites for Wastewater Treatment. *Macromol. Mater. Eng.* **2023,** *308*, 2200695. doi:10.1002/mame.202200695.

[3] Moradi, O.; Pudineh, A.; Sedaghat, S. Synthesis and Characterization of Agar/GO/ZnO NPsnanocomposite for Removal of Methylene Blue and Methyl Orange as Azo Dyes from Food Industrial Effluents. *Food Chem. Toxicol.* **2022,** *169*, 113412. doi:10.1016/j.fct.2022.113412.

[4] Kumar, V.; Bhatt, D.; El-Serehy, H.A.; Pandey, S. Gum Katira-Silver Nanoparticle-Based Bionanocomposite for the Removal of Methyl Red Dye. *Front. Chem.* **2023,** *10*, 959104. doi:10.3389/fchem.2022.959104.

[5] Gomase, V.; Doondani, P.; Saravanan, D.; Pandey, S.; Jugade, R.; A Novel Chitosan-Barbituric Acid Hydrogel Supersorbent for Sequestration of Chromium and Cyanide Ions: Equilibrium Studies and Optimization Through RSM. *Sep. Purif. Technol.* **2024,** *330*, 125475. doi:10.1016/j.seppur.2023.125475.

[6] Tran, N.B.T.; Duong, N.B.; Le, N.L. Synthesis and Characterization of Magnetic Fe_3O_4/Zeolite NaA Nanocomposite for the Adsorption Removal of Methylene Blue Potential in Wastewater Treatment. *J. Chem.* **2021,** *2021*, 1–14. doi:10.1155/2021/6678588.

[7] Kim, S.; Son, N.; Park, S.; Lee, C.; Pandey, S.; Facile, K.M. Fabrication of Oxygen-Defective ZnO Nanoplates for Enhanced Photocatalytic Degradation of Methylene Blue and In Vitro Antibacterial Activity. *Catalysts* **2023,** *13* (3), 567. doi:10.3390/catal13030567.

[8] Alahl, S.A.A.; Ezzeldin, A.H.; Ezzeldin, A.H.; Panday, S.; Kotp, H.Y. Synthesis of a Novel Photocatalyst Based on Silicotitanate Nanoparticles for the Removal of Some Organic Matter from Polluted Water. *Catalysts* **2023,** *13* (6), 981. doi:10.3390/catal13060981.

[9] Sadighian, S.; Tozihi, M. Synthesis, Characterization, and Dye Removal Applications of Graphene Oxide-Gold Nanocomposite. *Biointerface Res. Appl. Chem.* **2022,** *13*, 1–385. doi:10.33263/BRIAC134.385.

[10] Yaseen, M.; Farooq, S.; Khan, A.; Shah, N.; Shah, L.A.; Bibi, S.; Khan, I.U.; Ahmad, S. CuO-SiO_2 Based Nanocomposites: Synthesis, Characterization, Photocatalytic, Antileishmanial, and Antioxidant Studies. *J. Chin. Chem. Soc.* **2022,** *69*, 1637. doi:10.1002/jccs.202200182.

[11] Gassim, F.A.-Z.G.; MakkawiAsmaa, A.J.; Makkawi, M.; Hammadi, H. Synthesis and Characterization of ZnO-AgCl Nanocomposites and Applications in the Removal of Reactive Black 5H from Wastewater. *AIP Conf. Proc.* **2022,** *2547*, 040012. doi:10.1063/5.0112420.

[12] Mohammed, H.T.; Kadhim Alasedi, K.; Ruyid, R.; Abed Hussein, S.; Latif Jarallah, A.; Dahesh, S.M.A.; Q Sultan, M.; Salman, Z.N.; Bashar, B.S.; Kareem Obaid Aldulaimi, A. ZnO/Co_3O_4 Nanocomposites: Novel Preparation, Characterization, and Their Performance Toward Removal of Antibiotics from Wastewater. *J. Nanostructures* **2022,** *12*, 503. doi:10.22052/JNS.2022.03.003.

[13] Pandey, S.; Kim, S.; Kim, S.Y.; Kumar, D.; Kanfg, M. Fabrication of Next-Generation Multifunctional LBG-s-AgNPs@ g-C_3N_4 NS Hybrid Nanostructures for Environmental Applications. *Environ. Res.* **2024,** *330*, 125475. doi:10.1016/j.seppur.2023.125475.

[14] Ajel, M.K.; Al-Nayili, A. Synthesis, Characterization of Ag-WO_3/Bentonite Nanocomposites and Their Application in Photocatalytic Degradation of Humic Acid Inwater. *Environ. Sci. Pollut. Res.* **2023,** *30*, 20775. doi:10.1007/s11356-022-23614-4.

[15] Areej, F.; Munawar, T.; Mukhtar, F.; Nadeem, M.S.; Akbar, U.A.; Hakeem, A.S.; Iqbal, F. Synthesis and Characterization of rGO-Supported Mo/Cu Dual-Doped NiO Nanocomposite for the Elimination of Dye Pollutant. *Appl. Nanosci.* **2023,** *13*, 5641–5657. doi:10.1007/s13204-023-02786-6.

[16] Abinaya, M.; Rajakumaran, R.; Chen, S.-M.; Karthik, R.; Muthuraj, V. In Situ Synthesis, Characterization, and Catalytic Performance of Polypyrrole Polymer-Incorporated Ag_2MoO_4 Nanocomposite for Detection and Degradation of Environmental Pollutants and Pharmaceutical Drugs. *ACS Appl. Mater. Interfaces* **2019,** *11*, 38321. doi:10.1021/acsami.9b13682.

[17] Pourzare, K.; Farhadi, S.; Mansourpanah, Y. Graphene Oxide/Co_3O_4 Nanocomposite: Synthesis, Characterization, and Its Adsorption Capacity for Removal of Organic Dye Pollutants from Water. *Acta Chim. Slov.* **2017,** *64*, 945. doi:10.17344/acsi.2017.3642.

[18] Vithalkar, S.; Jugade, R.; Bambal, A.; Pakade, Y.; Pandey, S. Gamma-Sterilized Cow-Dung for Confiscation of Triphenylmethane Dyes from Water Bodies. *Environ. Prog. Sustain.* **2023,** *43*, e14262. doi:10.1002/ep.14262.

[19] Foroutan, R.; Peighambardoust, S.J.; Esvandi, Z.; Khatooni, H.; Ramavandi, B. Evaluation of Two Cationic Dyes Removal from Aqueous Environments Using CNT/MgO/$CuFe_2O_4$ Magnetic Composite Powder: A Comparative Study. *J. Environ. Chem. Eng.* **2021,** *9*, 104752. doi:10.1016/j.jece.2020.104752.

[20] Ma, H.; Shi, T.; Song, Q. Synthesis and Characterization of Novel PVA/SiO_2-TiO_2 Hybrid Fibers. *Fibers* **2014,** *2*, 275. doi:10.3390/fib2040275.

[21] Winey, K.I.; Vaia, R.A. Polymer Nanocomposites. *MRS Bull.* **2007,** *32*, 314. doi:10.1557/mrs2007.229.

[22] Mahar, Z.A.; Shar, G.Q.; Balouch, A.; Pato, A.H.; Shaikh, A.R. Effective and Viable Photocatalytic Degradation of Rhodamine B Dye in Aqueous Media Using CuO/PVA Nanocomposites. *New J. Chem.* **2021,** *45*, 16500. doi:10.1039/D1NJ02192C.

[23] Soltaninejad, V.; Ahghari, M.R.; Taheri-Ledari, R.; Maleki, A. Bifunctional PVA/ZnO/Agl/Chlorophyll Nanocomposite Film: Enhanced Photocatalytic Activity for Degradation of Pollutants and Antimicrobial Property Under Visible-Light Irradiation. *Langmuir* **2021,** *37*, 4700. doi:10.1021/acs.langmuir.1c00501.

[24] Malekkiani, M.; Heshmati Jannat Magham, A.; Ravari, F.; Dadmehr, M. Facilefabrication of Ternary MWCNTs/ZnO/Chitosan Nanocomposite for Enhancedphotocatalytic Degradation of Methylene Blue and Antibacterial Activity. *Sci. Rep.* **2022,** *12*, 1. doi:10.1038/s41598-022-09571-5.

[25] El-Shamy, A.G. An Efficient Removal of Methylene Blue Dye by Adsorption onto Carbon Dot@ Zinc Peroxide Embedded Poly Vinyl Alcohol (PVA/$CZnO_2$) Nano-Composite: A Novel Reusable Adsorbent. *Polymer* **2020,** *202*, 122565. doi:10.1016/j.polymer.2020.122565.

[26] Abdel-Mottaleb, M.; Khalil, A.; Karim, S.; Osman, T.; Khattab, A. High Performance of PAN/GO-ZnO Composite Nanofibers for Photocatalytic Degradation Under Visible Irradiation. *J. Mech. Behav. Biomed. Mater.* **2019,** *96*, 118. doi:10.1016/j.jmbbm.2019.04.040.

[27] Hussain, D.; Khan, S.A.; Khan, T.A.; Alharthi, S.S. Efficient Liquid Phase Confiscation of Nile Blue Using a Novel Hybrid Nanocomposite Synthesized from Guar Gum-Polyacrylamide and Erbium Oxide. *Sci. Rep.* **2022,** *12*, 14656. doi:10.1038/s41598-022-18591-0.

[28] Abebe, B.; Zereffa, E.A.; Murthy, H.A. Synthesis of Poly (Vinyl Alcohol)-Aided ZnO/Mn_2O_3 Nanocomposites for Acid Orange-8 Dye Degradation: Mechanism and Antibacterial Activity. *ACS Omega* **2020,** *6*, 954. doi:10.1021/acsomega.0c05597.

[29] Maijan, P.; Amornpitoksuk, P.; Chantarak, S. Synthesis and Characterization of Poly (Vinyl Alcohol-g-Acrylamide)/SiO_2@ZnO Photocatalytic Hydrogel Composite for Removal and Degradation of Methylene Blue. *Polymer* **2020,** *203*, 122771. doi:10.1016/j.polymer.2020.122771.

[30] Yaseen, M.; Humayun, M.; Khan, A.; Idrees, M.; Shah, N.; Bibi, S. Photo-Assisted Removal of Rhodamine B and Nile Blue Dyes from Water Using CuO–SiO_2 Composite. *Molecules* **2022,** *27*, 5343. doi:10.3390/molecules27165343.

[31] Sarwan, B.; Pare, B.; Acharya, A. Synthesis of Mn/NiO and Mn/BiOCl Nanoparticles for Degradation of Nile Blue Dye Contaminated Water Under Visible Light Illumination. *Part. Sci. Technol.* **2020,** *38*, 659–666. doi:10.1080/02726351.2019.1570991.

[32] Azharudeen, A.M.; Badhusha, A.; Khan, M.S.; Prabhu, S.A.; Kumar, P.V.; Karthiga, R.; Odeibat, H.A.; Naz, H.; Buvaneswari, K.; Islam, M. Solar Power Light-Driven Improved Photocatalytic Action of Mg-Doped CuO Nanomaterial Modified with Polyvinylalcohol. *J. Nanomater.* **2022,** *2022*, 2430840. doi:10.1155/2022/2430840.

[33] Rahman, S.; Khan, M.M.R.; Deb, B.; Dana, S.I.; Ahmed, M.K. Effective and Simplefabrication of Pyrrole and Thiophene-Based Poly (Py-co-Th)/ZnO Composites for Highphotocatalytic Performance. *S. Afr. J. Chem. Eng.* **2023,** *43*, 303. doi:10.1016/j.sajce.2022.11.010.

[34] Khan, A.; Noor, S.; Khan, M.S.; Khattak, R.; Malik, A.; Rahman, U.U.; Zekker, I.; Rahman, N.U.; Shah, L.A. Removal of Crystal Violet from Wastewater Using Synthesized Graphene Quantum Dots as Adsorbents: Kinetic Approach. *Int. J. Environ. Sci. Technol.* **2023,** *20*, 13219–13232. doi:10.1007/s13762-023-04881-1.

[35] Rahman, U.U.; Humayun, M.; Khan, A.; Saima Farooq, S.; Sadiq, M.; Bououdina, M.; Shah, N. Thermo-Chemical Modification of Cellulose for the Adsorptive Removal of Titan Yellow from Wastewater. *Molecules* **2023,** *28*, 3955. doi:10.3390/molecules28093955.

[36] Rehana, D.; Mahendiran, D.; Kumar, R.S.; Rahiman, A.K. Evaluation of Antioxidant and Anticancer Activity of Copper Oxide Nanoparticles Synthesized Using Medicinally Important Plant Extracts. *Biomed. Pharmacother.* **2017,** *89*, 1067. doi:10.1016/j.biopha.2017.02.101.